ENHANCING THE PRE-POLYMERIZATION COORDINATION OF 1-VINYLIMIDAZOLE IN BULK SOLUTION WITH IONIC LIQUID ADDITIONS

by

JACKIE RYAN HAMILTON

C. HEATH TURNE, COMMITTEE CHAIR
JASON E. BARA
HUNG-TA WANG
VINU UNNIKRISHNAN

A THESIS

Submitted in partial fulfillment of the requirements
for the degree of Master of Science in the
department of Chemical Engineering
in the Graduate School of
The University of Alabama

TUSCALOOSA, ALABAMA

2015

ABSTRACT

Recent experimental investigations have found that the photopolymerization of 1-vinylimidazole (VIm) can be significantly accelerated with the addition of lithium bis(trifluoromethylsulfonyl)-imide ($LiTf_2N$). However, a clear explanation for this phenomenon is lacking, and the underlying molecular level interactions in such a system are unknown. The two components, VIm and $LiTf_2N$, are soluble over a wide range of concentrations at ambient temperature, and if the fundamental behavior of this mixture can be clearly quantified, there are significant opportunities for tuning the polymerization dynamics, polymer structure, and properties. In this work, molecular dynamics simulations are used to model the underlying pre-polymerization structure of VIm/$LiTf_2N$ mixtures at several different concentrations. It is found that the Li^+ enhances the site-site interactions of key sites involved in the polymerization, and this is suggested to play a major role in the experimentally-observed enhancement of the polymerization behavior.

ACKNOWLEDGEMENTS

Financial support was provided by the National Science Foundation (CBET-1159397 and EEC-1358750).

CONTENTS

LIST OF TABLES

LIST OF FIGURES

Chapter 1. Introduction and Background

1.1 Motivation

There is a clear need to economically separate and capture CO_2 emissions from coal and gas fired power plants. In today's economy, coal and natural gas are very inexpensive sources of energy.[2] Although this may be perceived as a benefit to consumers, burning many megatons of coal and gas annually is beginning to have adverse effects on our planet.[3,4,5,6] The environmental effects of greenhouse gases have been known for quite some time.[3] Excess CO_2 and methane gases cause radiation from the sun to be trapped on earth, leading to incremental increases in the global temperature. Since the industrial revolution, atmospheric CO_2 levels have risen 25 percent.[7] The EPA has reported that in 2012 alone, 5.5×10^9 metric tons of CO_2 gas were released from energy production sources.[8] Only within the last 50 years has government regulation mandated that companies emitting pollutants be held accountable for the damage being done to the environment. Bills such as the Clean Air Act and the Clean Air Act Amendments have imposed regulations on the atmospheric emission of certain compounds. Compounds such as ammonia, nitrates and sulfates, which create acid rain and other damaging effects on the environment and agriculture have been efficiently and economically removed from flue gas for many years now.[9] Some of the removal technologies are even able to convert the unwanted emissions into resalable commodities. However until recently, there has not been such a strong push to remove CO_2 from flue

gas. A few reasons for this may be that the effects of global warming have not been as broadly accepted in the past, or that there have not been economical technologies for removing CO_2 from flue gas.[10] However, recent domestic governmental regulations have placed strict mandates on CO_2 emissions. In 2014, President Obama passed a plan developed by the EPA to begin implementing regulations for carbon emissions in the United States.[11] In future years, in order for coal and gas burning plants to be able to compete with nuclear and renewable energy sources as well as the new regulations taking place, engineers must develop an inexpensive and efficient method for separating and capturing CO_2 from flue gas.[2]

1.2 Methods of CO_2 Removal

It is possible with today's technology to remove the regulated amounts of CO_2 from flue gas. The problem is that the process economics and efficiency of these processes are not viable on large scales. The current leading industrial technology for CO_2 capture is through chemical absorption with aqueous monoethanol amine (MEA), which is composed of approximately 18% MEA.[12] However, using chemical absorption with MEA to remove CO_2 gas in coal and gas fired power plants can reduce the final electricity output by up to 20 percent. This is an enormous energy penalty requiring increased fuel consumption and large increases in energy costs to consumers. The cost of the energy to remove about 90 percent of CO_2 from post combustion flue gas is around $40 per metric ton. However, this cost does not consider transportation, storage, and solvent replacement.[13]

Since the current technologies for CO_2 separation and capture are economically unfeasible, other methods have been proposed for removing CO_2. Chemical absorption technologies use solvents such as MEA (which chemically reacts with CO_2), while Selexol® physically absorbs CO_2. In both cases, the regeneration steps require high temperatures and/or low pressure to release CO_2 from the solvent.[14] The process for either regeneration approach requires a lot of expensive equipment, including stripper columns, pumps, and heat exchangers. Therefore implementing these types of systems requires a very large initial cost, and because of the pressure drop and evaporative solvent losses, operation costs can also be significant.

There are some more radical approaches for sequestering CO_2 from flue gas. One interesting, yet currently unfeasible, method for extracting CO_2 from flue gas is cryogenic separation. By cooling the gases, separation can occur based on the difference in boiling points. This process has been commercially used for liquefying CO_2 from a high >90% CO_2 source.[15] However, since typical post combustion flue gas contains such a low overall concentration of CO_2 (as well as other SO_X and NO_X compounds), the energy cost for this method far exceeds equivalent separation with MEA absorption.[16] Major advances in cooling efficiency are required in order for this method to become competitive. Another slightly more practical option is to design plants to use O_2 rich combustion sources by using pure O_2 instead of air that is only ~21% O_2. This process change would raise the partial pressure of CO_2 in the flue gas making existing sequestration methods much more economical.[16] The main challenge with this approach is that many of the existing coal and gas fired plants are not design to handle the increased combustion temperature that O_2 rich combustion would create.[12] Moreover, the

cost to retrofit existing power plants to handle these harsher conditions would be equivalent to the cost of a completely new facility.

Physical adsorption onto porous materials is another potential avenue for CO_2 capture. If flue gas is passed through a packed bed of a high surface area material such as activated carbon,[17] CO_2 molecules can be selectively adsorbed to the pore surface. One challenge with this approach is the finite loading capacity of the adsorbent material. Within a short period of operation time, the pores can become saturated with CO_2 and need to be replaced or regenerated. This makes the CO_2 capacity of the sorbent material very important when assessing the capital and operating cost of such a method.[18]

Another promising alternative is using membranes for removing CO_2 from flue gas. Membrane separation can be achieved by selectively absorbing and diffusing CO_2, while preventing other gasses (such as nitrogen or water vapor) to pass through the porous media. This method of separating CO_2 from post combustion exhaust gas potentially requires less energy, there are no sorbents to regenerate, and since there are no moving parts, the maintenance costs can be minimized.[19] In addition to the separation performance of the membrane, there are also other practical issues that must be considered. For instance, the pressure drop resulting in the use of membrane separation should be comparatively low compared to other gas purification methods.[9] Some examples are listed in Table 1, which should serve as benchmarks for viable membrane performance. In addition to pressure drop, the durability of the membrane is a critical issue. Performance must be able to be sustained for an extended period of time, regardless of swings in operating temperature, the existence of other trace components, or varying flow rates.

Table 1. Comparison of pressure drops for typical gas purification systems used to treat industrial post-combustion exhaust gas

Gas Removed	Method	Pressure Drop (kPa)
N/A	Open Exhaust column	1.7 [20]
NO_x	SCR (Packed Bed)	1.2 [21]
SO_x	Wet FGD (Scrubber)	2.5 [20]
CO_2	Chemical Absorption	1.3 [22]

One of the major limitations of current membrane materials is that reaching an acceptable CO_2/N_2 selectivity is very difficult. In order to achieve the necessary level of CO_2 separation, the CO_2/N_2 selectivity must be a minimum of 200. However, the best existing membrane materials (using precious metal catalysts, such as palladium) are only able to achieve a CO_2/N_2 selectivity of 100.[23] However, with developments in imidazole-based polymers and ionic liquids, there are opportunities to synthesize novel membrane materials that are inexpensive to produce at large volumes, yet have the potential to yield high selectivities and low pressure drops for CO_2 separation from industrial combustion exhaust gas.

1.3 Ionic Liquids

An ionic liquid at the most basic description is a liquid composed completely of ions. By this definition, all salts heated to achieve a liquid state would be considered an ionic liquid. However, most salts have very high melting temperatures, and these "molten salts" are not ideal for most industrial processes. Ionic liquids were first studied over 100 years ago, and one of the earliest documentations of ionic liquids was the "red-oil" that forms as a result of a Friedel-Crafts reaction.[24]

The chemical and physical properties of ionic liquids can be widely varied, based on the cation-anion combination.[25] This vast parameter space has motivated many researchers to synthesize and explore the properties of new ionic liquids. While the thermophysical and chemical properties of ionic liquids can be tuned for specific applications, there exist some general properties that are true of almost all ionic liquid compounds. One of the most distinct properties is a very low vapor pressure. Many ionic liquids have vapor pressures so low that they are considered negligible compared to that of a solid. For industrial applications, this property can provide unique benefits, since evaporative solvent losses can be minimized. Furthermore, many room temperature ionic liquids (RTILs) have melting temperatures below 303 K, and they do not experience chemical decomposition until temperatures of 600-700 K.[26]

Another universal property of ILs is that they can dissolve a wide variety of compounds including both polar and non-polar species, and organic and inorganic species. Moreover, ILs can be tuned to serve as selective solvents for compounds such as alcohols, aromatics, polymers, and even certain gases, such as CO_2. Outside of separation

technologies, ionic liquids can serve as electrically conductive[27] solvents, and due to their structure, they can also possess high ionic conductivity.[28] This opens up potential applications in fuel cells, batteries, sensors, and other electrochemical devices. Depending on the ion combination, there are many other additional applications of ILs in reaction engineering and other industrial processes.

Recent studies performed by a group at Notre Dame have found that imidazolium-based ILs (such as 1-ethyl-2-methyl imidazolium (emim) and bis(trifluoromethylsulfonyl)-imide ($LiTf_2N$)) are surprisingly good at dissolving CO_2.[29] Following early indications that IL compounds can dissolve CO_2, Gonzalez-Miquel, et al. performed COSMO-RS simulations of 1-butyl-2-methyl imidazolium (bmim) Tf_2N and other imidazolium-based IL combinations to predict CO_2/N_2 selectivity. Unfortunately, they found that these mixtures were well below a CO_2/N_2 selectivity that would be economically acceptable.[30] However, other groups have shown that polymer membranes of alkyl imidazolium Tf_2N can reach the upper bound on the Robeson Plot,[31] surpassing the performance of other polymers. Another group reported that certain functionalized imidazoliums can even drive CO_2/N_2 selectivity beyond the current upper bound of performance.[32]

These initial encouraging results have motivated us to pursue other novel imidazole-based polymer membranes. One potential candidate material is polyvinylimidazole (poly-VIm). Poly-VIm is a polymer with an imidazole pendant, which can be produced in a bulk solution via radical photopolymerization. This polymer has received a great deal of attention in recent studies and has been used for many applications, such as coating electrodes,[33] fuel cell membranes,[34] and separations

applications including CO_2 adsorption[35,36] and the adsorption of metal ions.[37] One of the challenges of producing poly(vinylimidazole) in bulk solution is that the polymerization is very slow, with a conversion of around eighty percent,[38] and this behavior is attributed to mass transport limitations in such a viscous solution.[38] Overcoming the mass transport limitations in bulk photopolymerization has been a critical issue in recent polymer research,[39,40] and the wide range of applications for poly(vinylimidazole) make it a strong candidate for further research. Much of the past work on this topic has dealt with polymerizing monomers in conventional solvents and salts to explore polymerization rates[41,42]; however, due to their unique properties, recent research has considered ionic liquids (ILs) as effective additives for such reactions.[43,44] The use of ionic liquids in radical polymerization has been found to increase propagation rates and decrease termination rates leading to an overall increase in polymer conversion.[45] Past studies have explored the polymerization of methyl methacrylate (MMA), acrylonitrile, and VIm with the addition of Lewis acids with different metal cations.[46,42,47] These studies have suggested that certain metals are likely to form a ligand complex with monomers and smaller polymer chains in solution that can help to coordinate specific molecules, leading to increased polymerization rates. Because of its high melting temperature, $LiTf_2N$ is not a room temperature IL but because of the complex formed with the metal cation and monomer, adding $LiTf_2N$ to specific solutions forms an ionic liquid complex. The addition of $LiTf_2N$ has been considered for enhancing the polymerization of methyl methacrylate (MMA)[40] and poly(vinylimidazole).[38] Both studies indicate an increase in reaction rate and monomer conversion.

Motivated by several of these previous experimental studies, we use molecular dynamics simulations to explore the underlying molecular interactions responsible for the reaction enhancement in mixtures of 1-vinylimidazole (VIm) in bulk solution with $LiTf_2N$. In computational studies, ionic liquids have been a popular topic for quite some time, and $LiTf_2N$/IL mixtures have been modeled by others in the past.[48,49,50] This work attempts to find simulation parameters for a fixed charge model of $LiTf_2N$ that will allow accurate simulations of pure $LiTf_2N$, $LiTf_2N$ in water, and $LiTf_2N$ in a solution of VIm, so that we can clarify the coordination environment of the VIm monomers.

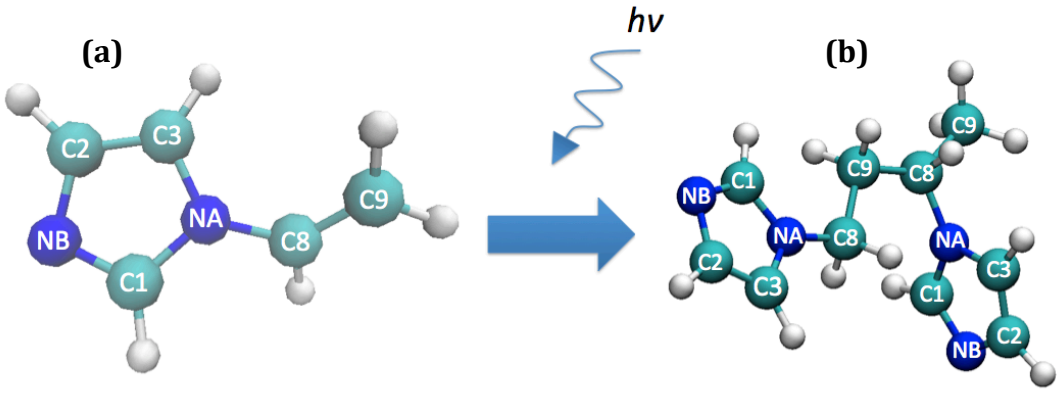

Figure 1 Illustration of the photopolymerization of **(a)** VIm to **(b)** a vinylimidazole dimer, including the labels of individual sites. The reaction primarily occurs through the C8-C9 sites.

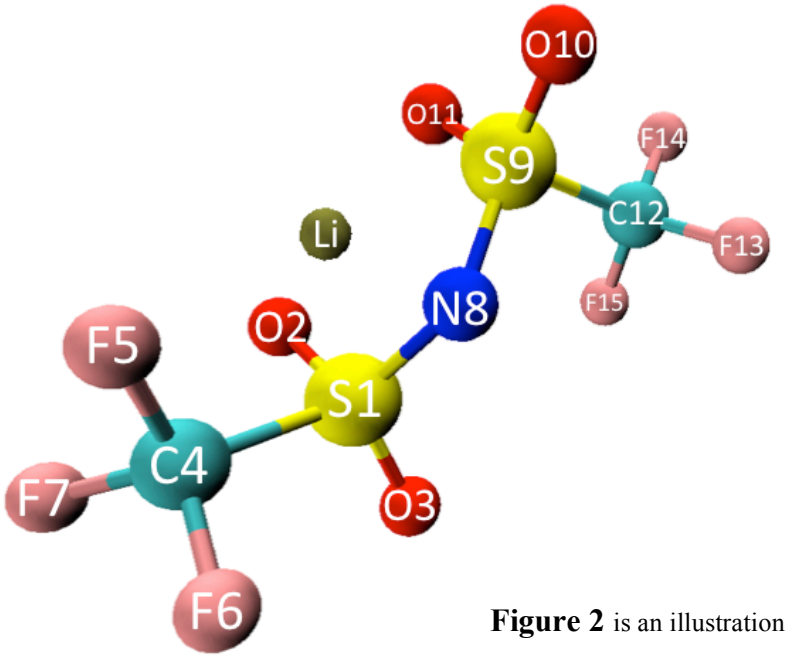

Figure 2 is an illustration of $LiTf_2N$.

By comparing experimental properties to those calculated from the simulations of VIm in solution with $LiTf_2N$, accurate models are generated and analyzed and yield a better understanding of the physical mechanism that allows polymerization of polyvinylimidazole to overcome its mass transport limitation and achieve much higher conversions. In this study, eight mixtures of VIm and $LiTf_2N$ were modeled using molecular dynamics simulations with molar ratios of VIm to $LiTf_2N$ ranging from 1:1 to 10:1. These ratios were chosen based on the opportunity to compare with experimental density data,[38] which were used as initial benchmarks. By comparing experimental properties to those calculated from the simulations of VIm in solution with $LiTf_2N$, refined molecular models are generated and used to identify the key interactions is these mixtures, in order to understand the polymerization enhancement.

Chapter 2. Simulation Methods

2.1 Computational Background

The goal of this work was to clarify the molecular-level structural data about the VIm/LiTf2N system. To set up these simulations, we first needed to find an optimized geometric structure, so that accurate calculations of the structural coordination of molecules could be determined. By determining the lowest energy configuration of a molecule, we can more accurately simulate the behavior of the system, and more correctly assign fixed partial charges to a molecule. Although fixed charges do not exist in nature, this assumption allows for faster calculations with only a slight compromise in accuracy. Finally, using the calculated initial geometry and partial charges, simulations were constructed to explore how the molecules interact and coordinate with each other. This work involved two main computational methods, Density functional theory (DFT) with natural bond orbital population analysis (NBO), and molecular dynamics (MD). DFT analysis is a quantum mechanical based calculation, and it needs no experimental parameters. Unlike other quantum mechanical methods, DFT directly accounts for the electron correlation, both accurately and efficiently. Natural bond orbital (NBO) population analysis is a method for approximating partial charges of atoms in a molecule. There are multiple methods for population analysis, or assigning charge distribution. It should be understood that partial charges are an approximation of the highest probability

of electron density around atoms in a molecule. Mulliken population analysis is the default Gaussian method. Although it is computationally efficient, it tends to be very inaccurate. This method divides charges between atoms that share electrons by assuming that all elections are equally shared. In comparison, the natural bond orbital (NBO) population analysis provides a more accurate approximation, assigning partial charges by classifying orbitals in non-bonding, natural atomic orbitals, and natural bonding and anti-bonding orbitals. This method is more computationally expensive, and for large molecules can be very time intensive, but partial charges generated with this method are more accurate.

Molecular Dynamics has been one of the workhorses of molecular simulations since the dawning of the computer. Using an IBM 704, Alder and Wainwright observed 32 hard spheres dance around a box with attractive potentials, followed by Rahman in 1964 who applied Lennard-Jones potentials to 864 argon atoms. Since these simple beginnings, there have been exponential leaps in computing power and algorithm development. Now molecular dynamics (MD) simulations methods are used to calculate equilibrium properties (density, pressure, temperature, free-energy, specific heat) and transport properties (self-diffusion, conductivity, viscosity) in systems with millions of atoms. Using classical mechanics and integration of Newton's equation of motion, MD simulations march forward in time by updating positions and velocities.

Once these simulations are performed, the results can be directly compared to experimental measurements, and like experiments, many of the errors that can occur with simulated results are related to an incorrectly prepared sample, too short of a measurement, or not measuring the correct property. However, if samples are prepared

correctly, the parameters are accurate, and the system is large enough and allowed to run for an appropriate amount of time, simulations can provide much of the same information that could be obtained in an experimental lab.

2.2 Simulations Details

The simulations in this work were performed with GROMACS version 4.6.5[51] and following equilibration, production was allowed run for 10^6 steps with a time step of 0.001 ps, for a total simulation time of 1.0 ns. Longer simulations were not necessary in this case; and data from simulations of 10 ns matched that of the 1.0 ns simulations. Pressure was maintained at 1 bar using a Parrinello-Rahman barostat,[52] and temperature was fixed using a Nose-Hover thermostat.[53] The method for reaching equilibrium in well mixed simulations was to start by placing molecules randomly in a box and raising the temperature in a NVT simulation to 2000 K. Pressure was then raised in a NPT simulation to 120 bar. After snapshots of the simulation appeared to contain a well-mixed solution, temperature was allows to slowly drop to 303 K and pressure was relaxed to 1 bar using NPT simulations. The simulation was determined to have reached equilibrium once the system at 303 K and 1 bar was observed to have a constant total energy.

The particle-mesh Ewald (PME)[54] was used for long-range electrostatic interactions with a Coulomb cut-off of 0.9 nm and Fourier spacing of 0.12 nm^{-1}. Site-site interactions were cut off at 0.9 nm and standard tail corrections for energy and pressure were used to account for long-range interactions.[55] Parameters for all simulated molecules were described using an OPLS all atom force field[56] and other sources[57]. Fixed

bond lengths were used for all molecules, and this constraint is expected to result in a negligible loss in accuracy[58]. The Lennard-Jones potential was used to describe the interactions between atoms, and Lorentz-Berthelot mixing rules used to account for unlike pairs interactions, unless otherwise specified.

The simulations used a fixed charge model to represent electrostatic interactions. In order to obtain these partial charges, the electronic structures of VIm and the IL anions were calculated with Gaussian 09.[59] In the first step, DFT was used to find a minimum energy configuration and were conducted using the B3LYP functional[60] and the 6-31 g++(d,p) basis set. This was followed by a NBO population analysis[61] at the MP2/6-311++g(3d,3p) level of theory. In order to refine the electrostatic charges to be used in the MD simulations, the NBO charges for VIm from MP2 calculations were scaled by a factor of 0.8, as well as the charges on the IL cation and anion model (as listed in Tables 1 and 2). Although there are more sophisticated methods for quantifying partial charges in ILs, a fixed scaling factor of 0.8 tends to improve the kinetic and thermodynamic properties (versus using integer charges on the anions and cations). This same scaling factor has also been shown to improve agreement with imidazole-based molecules, when comparing simulated and experimental thermophysical properties. Recent studies have shown that scaling ion charges can help account for the effect of polarizability, and that it is not always necessary to have an integer charge when simulating ion pairs.[62] Preliminary simulations with integer charges resulted in densities that were significantly higher than the experimental data for the corresponding mixtures. Tf_2N was modeled as a 15 site charge based models from Zhao et al,[63] and PF_6 and BF_4 were assigned partial

charges based on models in previous studies.[64] VIm was modeled as 13 sites and is charge neutral.

Chapter 3. Results

The results are presented in three main parts. First, we benchmark simulation data to experimental data of pure components and mixtures. This allowed us to slightly refine our intermolecular potential model. Next, we analyze the local coordination of the VIm monomers with respect to the addition of varying amounts of $LiTf_2N$. Finally, we extend our study by examining the local VIm coordination behavior with respect to three other similar ionic liquids, including $NaTf_2N$, KTf_2N, $Mg(Tf_2N)_2$, $LiPF_6$, and $LiBF_4$.

Table 2. A compilation of the intermolecular parameters used for modeling VIm. The partial charges for VIm in this table were calculated using NBO population analysis and then scaled by a factor of 0.8. The net charge of each molecule is shown in parenthesis.

site	charge (e^-)	epsilon (kJ/mol)	sigma (nm)
	VIm (0.0e^-)		
C1	0.260	0.293	0.355
C2	-0.013	0.293	0.355
C3	-0.035	0.293	0.355
NA	-0.406	0.711	0.325
H5	0.151	0.126	0.242
H6	0.161	0.126	0.242
NB	-0.446	0.711	0.325
C8	0.068	0.318	0.355
C9	-0.325	0.318	0.355
H10	0.146	0.126	0.242
H11	0.153	0.126	0.242
H12	0.144	0.126	0.242
H13	0.142	0.126	0.242

Table 3. A compilation of the partial charges used for modeling the anions and cations. The partial charges in this table were based on previous studies and then scaled by a factor of 0.8e.[63, 64]

site	charge (e^-)	epsilon (kJ/mol)	sigma (nm)
	Tf_2N (-0.8e^-)		
S1	0.816	1.046	0.373
O2	-0.424	0.879	0.311
O3	-0.424	0.879	0.311
C4	0.280	0.276	0.368
F5	-0.128	0.222	0.310
F6	-0.128	0.222	0.310
F7	-0.128	0.222	0.310
N8	-0.528	0.711	0.341
S9	0.816	1.046	0.373
O10	-0.424	0.879	0.311
O11	-0.424	0.879	0.311
C12	0.280	0.276	0.368
F13	-0.128	0.222	0.310
F14	-0.128	0.222	0.310
F15	-0.128	0.222	0.310
	Hexafluorophosphate (-0.8e^-)		
P	1.072	0.8368	0.3927
F	-0.312	0.2552	0.3276
	Tetrafluoroborate (-0.8e^-)		
B	0.941	0.3928	0.3760
F	-0.435	0.2552	0.3276
	Cations		
Li	0.80	0.076	0.223
Na	0.80	0.012	0.350
K	0.80	0.0014	0.493
Mg	1.60	3.66	0.164

3.1 Pure $LiTf_2N$

To evaluate the performance of the $LiTf_2N$ force field, a pure $LiTf_2N$ system was used to compare simulated and experimental densities. At room temperature $LiTf_2N$ is a solid; its melting temperature is 507K,[65] so to evaluate our intermolecular parameters, simulated densities of pure $LiTf_2N$ were compared to an experimental data set over a range of liquid conditions.[1] The simulated densities for pure $LiTf_2N$ using the original parameter set[56,63] were 6-7% higher than the experimental values over the temperature range explored. In order to improve the simulation results, a number of different moderate adjustments to the interactions were explored (different charge scaling values, alternate cross-term mixing rules, etc.). Ultimately, the best performance was found by scaling all of the Lennard-Jones sigma values by 1.05, which led to an overall decrease in the system density. These scaled sigma values are shown in Tables 1 and 2. As shown in Figure 3, the simulated densities using the refined parameters for $LiTf_2N$ fall within less than 1% of the experimentally measured densities. Similar methods have been used for refining simulation parameters for ionic mixtures.[66] While more comprehensive model evaluations may be possible with additional experimental data, an improvement in the density prediction is interpreted to be a worthwhile outcome, especially considering the structural information probed in the current study. As more experimental data becomes available, additional benchmarking studies are anticipated to lead to further model improvements.

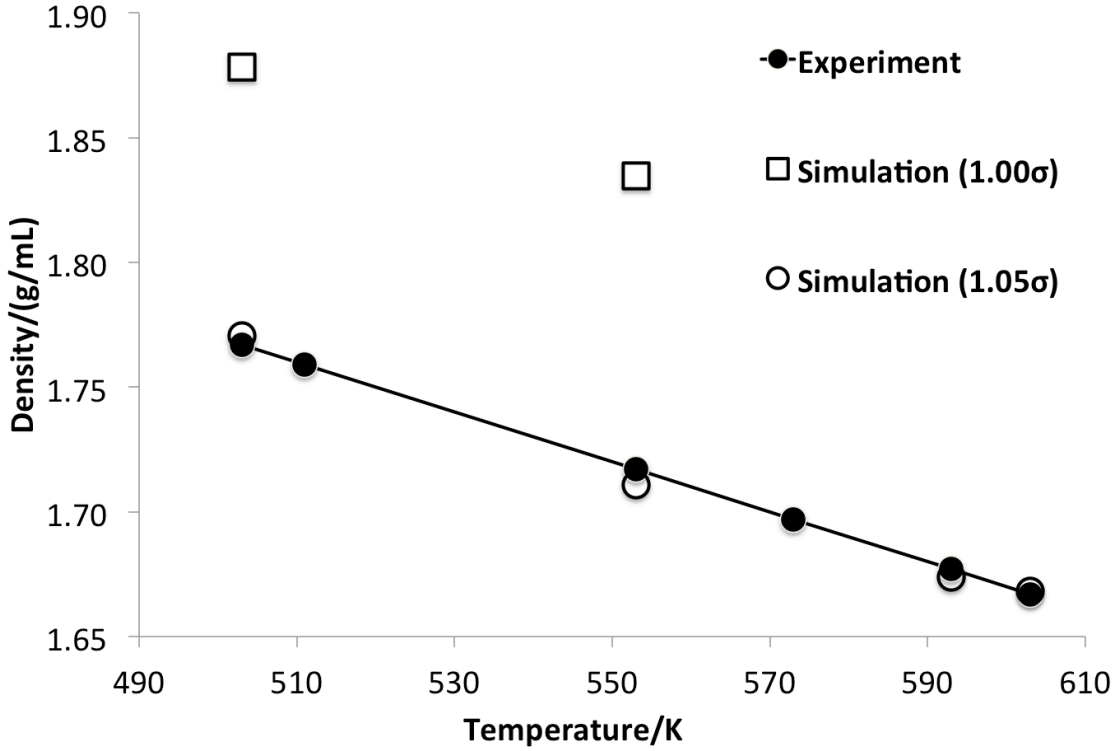

Figure 3. Density of pure $LiTf_2N$ with respect to varying temperature of simulations with original and with scaled Lennard-Jones potentials (shown in Table 2). By scaling the sigma value for each atom by 1.05, the simulated density is consistent with the experimentally measured density.[1]

Following the parameter refinement, simulations of $LiTf_2N$ in water were also conducted, in order to perform additional benchmarking against experimental densities. The refined charges and LJ parameters listed in Table 2 were used for $LiTf_2N$, and the water molecules were described by the SPC intermolecular potential.[67] Figure 4 shows that the comparison between simulation and experimental densities is very good (<2% error) over a fairly broad range of $LiTf_2N$ concentrations.

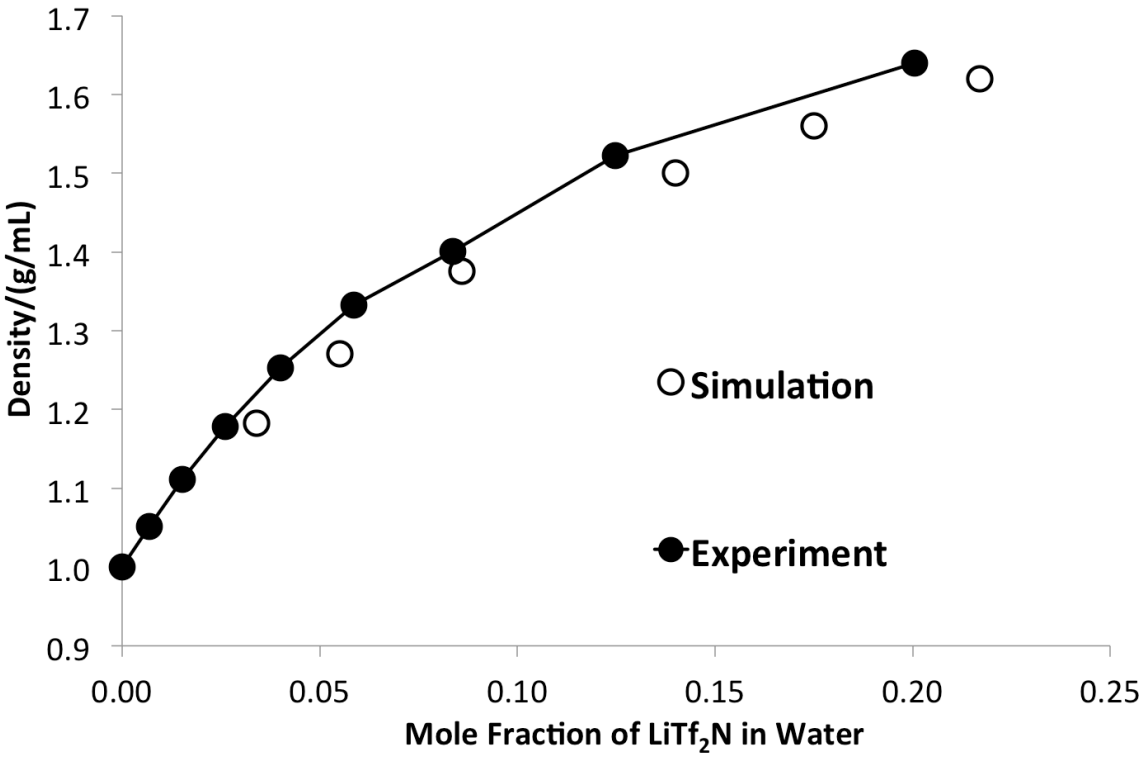

Figure 4. Comparison of experimental and simulation densities of mixtures of $LiTf_2N$ and SPC water at a temperature of 303 K.

3.2 $LiTf_2N$ in VIm

After the intermolecular parameters for $LiTf_2N$ were benchmarked against the pure liquid and against aqueous $LiTf_2N$ mixtures, simulations were performed for the VIm + $LiTf_2N$ mixtures. Before performing detailed analysis of the liquid structure and site-site interactions, the simulated densities were again compared against experimentally-measured densities.[38] At a fixed temperature of 303 K, the mole fraction

of $LiTf_2N$ in the VIm monomers was varied from a value of approximately 0.09 to a value of 0.25, with the density comparison shown in Figure 5. The simulated densities are consistently higher than the experimental values by approximately 5%, but this is an improvement over the results obtained using the original parameters for $LiTf_2N$, which led to discrepancies of close to 10% (data not shown). In lieu of any other experimental benchmarks for this mixture, we were not motivated to pursue any further parameter alteration, as this error falls within the level of accuracy that one might expect using purely predictive methods of force field generation.[66] This issue may be revisited in the future, as additional experimental data would allow for further quantitative improvement.

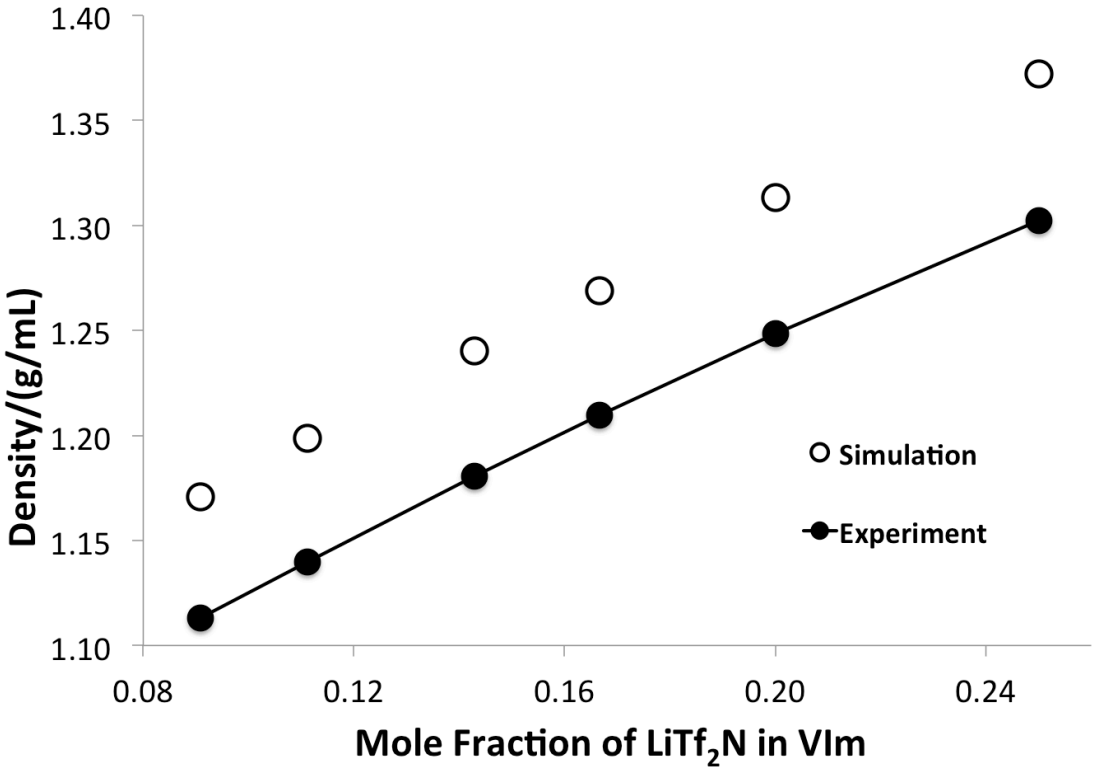

Figure 5. Density profile with respect to mole fraction of $LiTf_2N$ in VIm at a temperature of 303 K.

3.3 Pre-Polymerization Molecular Structure

Following the initial experimental benchmarking of the simulation models, radial distribution analysis was conducted to explore the coordination of the molecules in the system. For this study, the two most important pair interactions are: (a) the correlation between the carbons on the alkene functional group where polymerization takes place (C8 and C9 sites); and (b) the interactions between Li^+ and the NB nitrogen on the exterior region of the imidazole ring in VIm. In experiments, the addition of $LiTf_2N$ raised both reaction rate and conversion.[38] In our simulations, we find that as the concentration of $LiTf_2N$ in the VIm mixture is increased (up to a mole fraction of 0.50), there is a higher probability of finding the polymerizing carbons (C8 and C9) in close proximity.[48] When comparing the pure VIm monomers to the solution with 50 mol% $LiTf_2N$, the height of the first peak in Figure 6 shifts from approximately 1.17 to a value of 1.52, indicating a significant enrichment in the local C8-C9 coordination.

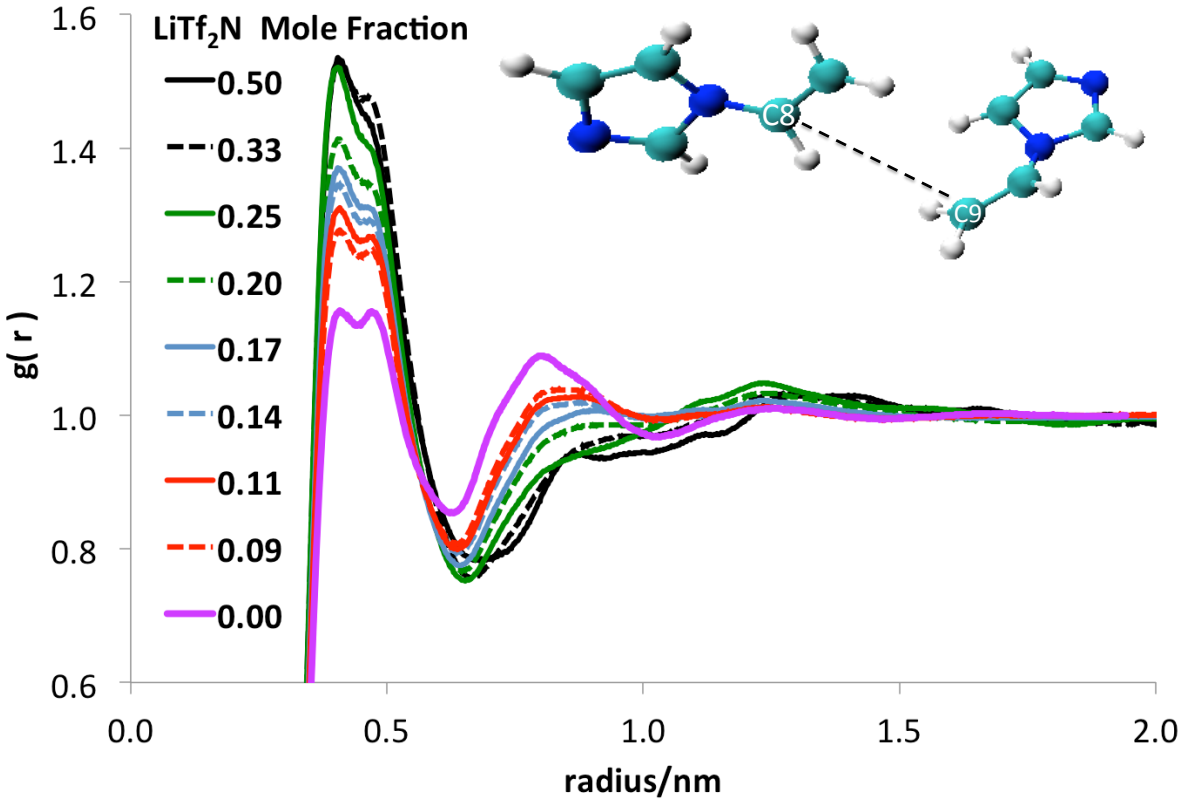

Figure 6. Comparison of radial distribution functions of systems with varying mole fractions of $LiTf_2N$ in VIm. The site-site radial distribution function is defined between the C8 and C9 carbons on the alkene group of VIm.

To further explore the direct effect of the $LiTf_2N$ on the pre-polymerization structure of the VIm monomers, we analyzed the local coordination of the VIm molecules around the Li^+ cations. To determine a reasonable cut off for this calculation (i.e., the extent of first coordination shell), a radial distribution function of the Li^+ and NB sites (shown in Figure 1) was calculated, and Figure 7 illustrates that a cutoff distance of 0.3 nm is a reasonable estimate of the first coordination shell.

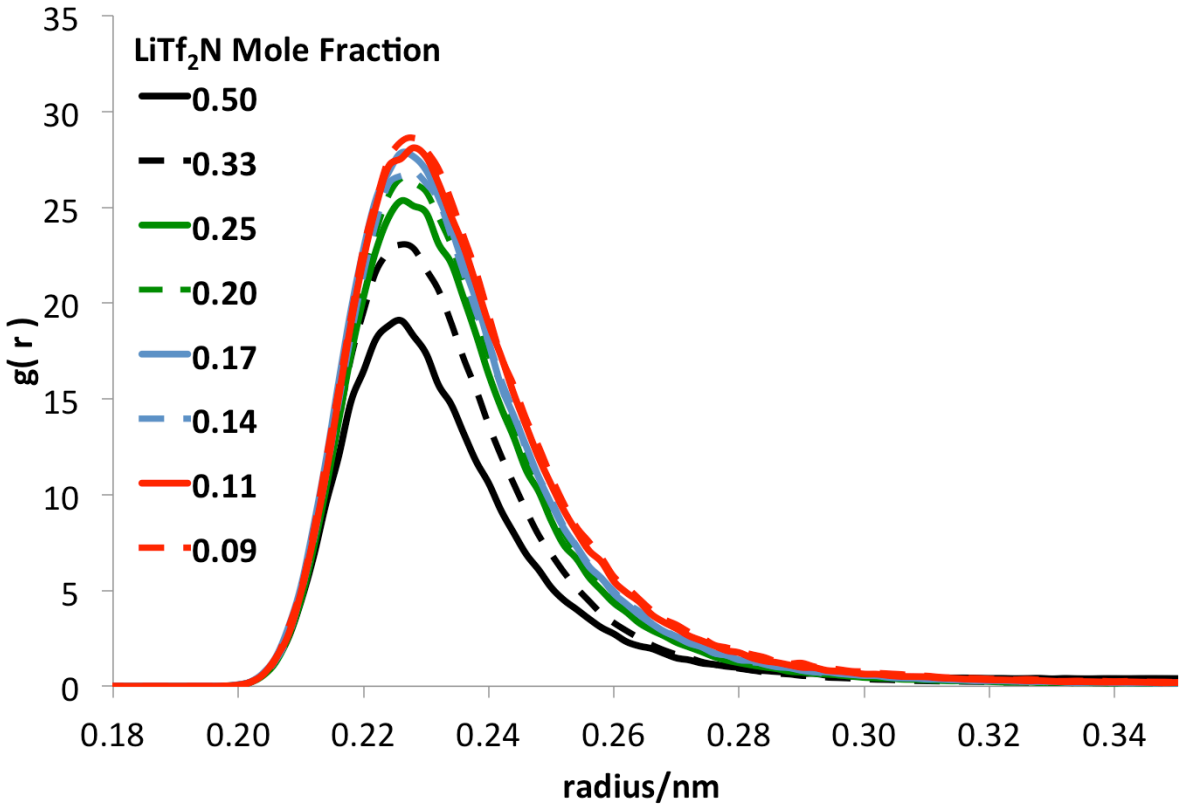

Figure 7. Radial distribution function of Li-NB at different mole fractions of $LiTf_2N$ in VIm at 303K.

The coordination of VIm about the Li^+ cations was calculated for all concentrations of $LiTf_2N$ in VIm. This local coordination environment was then compared to infrared spectroscopy absorbance data taken from experimental samples of these same solutions. Figure 8 shows the overlay of the experimental spectroscopy data and the simulated predictions of the local Li^+ coordination environment. While there is not a quantitative correlation between these two separate sources of data, the experimental and computational perspectives tend to mimic the same trend, especially when examining the 1:1 and 2:1 interactions.

Thus, one might infer that the interaction measured through IR spectroscopy is reflecting the local coordination of the VIm and Li^+ interaction. While this observation is not conclusive, it can be more rigorously explored in future studies of similar systems.

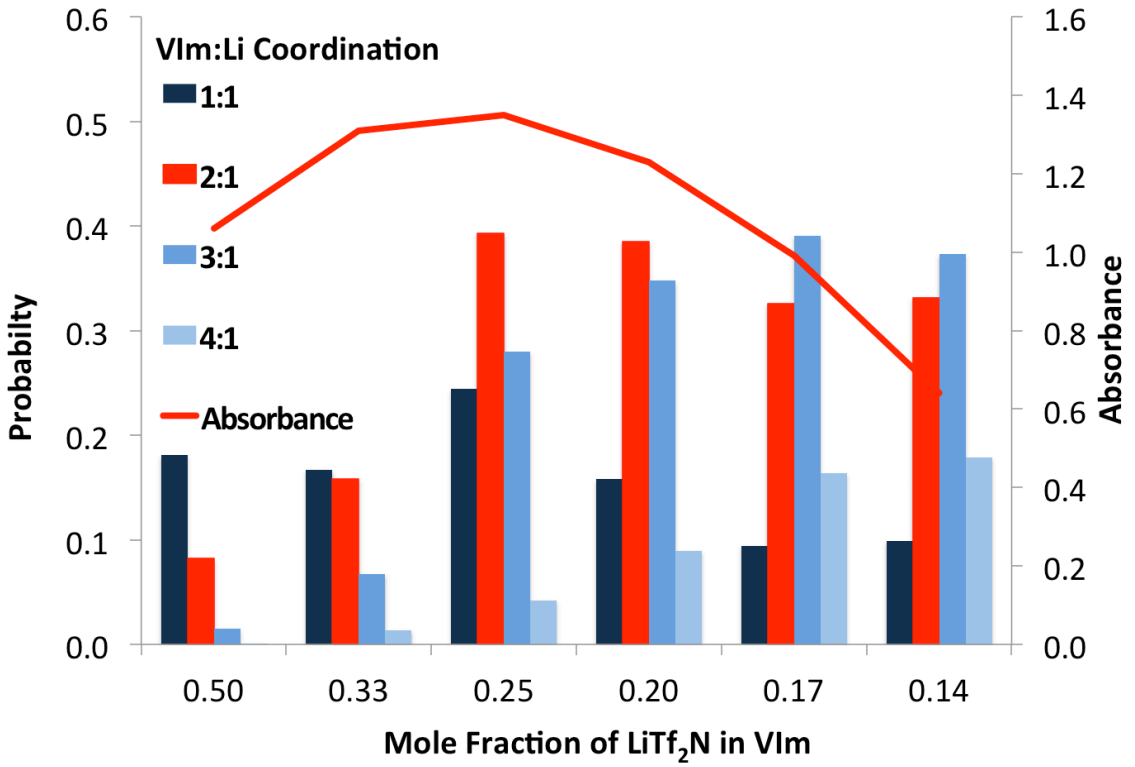

Figure 8. Comparison of coordination of VIm about the Li^+ cation of solutions with different mole fractions of $LiTf_2N$ at 303 K. The plot above shows that for the 2:1 interaction, the simulated probability data is consistent with experimental absorbance data.

3.4 Comparison with Other Ionic Liquids: $NaTf_2N$, $LiPF_6$, and $LiBF_4$

In order to broaden our investigation and explore the role of other IL solvents on the VIm pre-polymerization structure, three other similar ILs were considered: $NaTf_2N$, $LiPF_6$, and $LiBF_4$. Since experimental data was available in the literature,[1] the simulated

densities of pure $NaTf_2N$ were compared to experimental data before analyzing the coordination effects. For consistency, the same Lennard-Jones scaling procedure for $LiTf_2N$ was used to modify the original $NaTf_2N$ model (i.e. scaling all of the sigma values by 1.05), and the resulting parameters are listed in Table 2. The Lennard-Jones parameters for $LiPF_6$ and $LiBF_4$ were not modified from the original source[64] as they were derived for a eutectic mixture similar to the one used in this work.

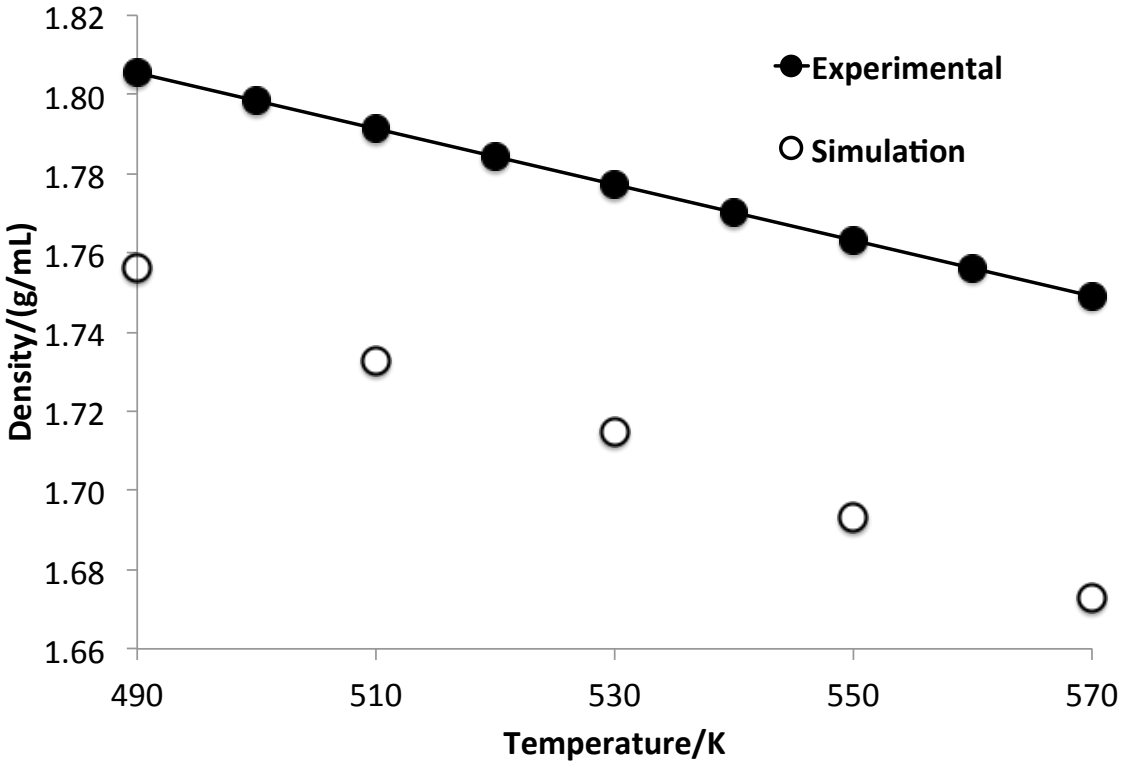

Figure 9. Density of pure $NaTf_2N$ with respect to temperature using the scaled Lennard-Jones potentials shown in Table 2 and experimentally measured densities taken from the literature.[1]

The simulated densities of $NaTf_2N$ were found to fall within 2-3% of the experimental densities,[1] which was deemed acceptable.[66]

Once again, the radial distribution functions show how VIm coordinates in a mixture with $NaTf_2N$. Like with $LiTf_2N$, as the concentration of $NaTf_2N$ increases, the peak heights in the g(r) plot also increase, meaning the local coordination of the C8 and C9 VIm sites are also increased. Figure 10 however, directly compares 3:1 VIm to IL mixtures of both $LiTf_2N$ and $NaTf_2N$. The graph shows that there is a slightly higher local concentration of VIm in the solution containing $LiTf_2N$. One possible reason for this is shown in Figure 11, which is the radial distribution function of Na-NB. The peak between Na^+ and NB occurs at a greater separation distance than between Li^+ and NB. This is due to the larger size of the Na^+ cation, which has an atomic radius of 102 pm compared to Li^+, which has an atomic radius of 76 pm.[68] As observed with the Li^+ cation, VIm also forms a complex with the Na^+ cation, but the characteristics are somewhat different. Coordination calculations (Figure 12, this time using a cut-off of 0.4 nm), show that VIm has a higher coordination about Na^+ than it does with Li^+. Once again, this may be due to the fact that Na^+ is a larger atom and therefore has more surface area for coordinating monomers.

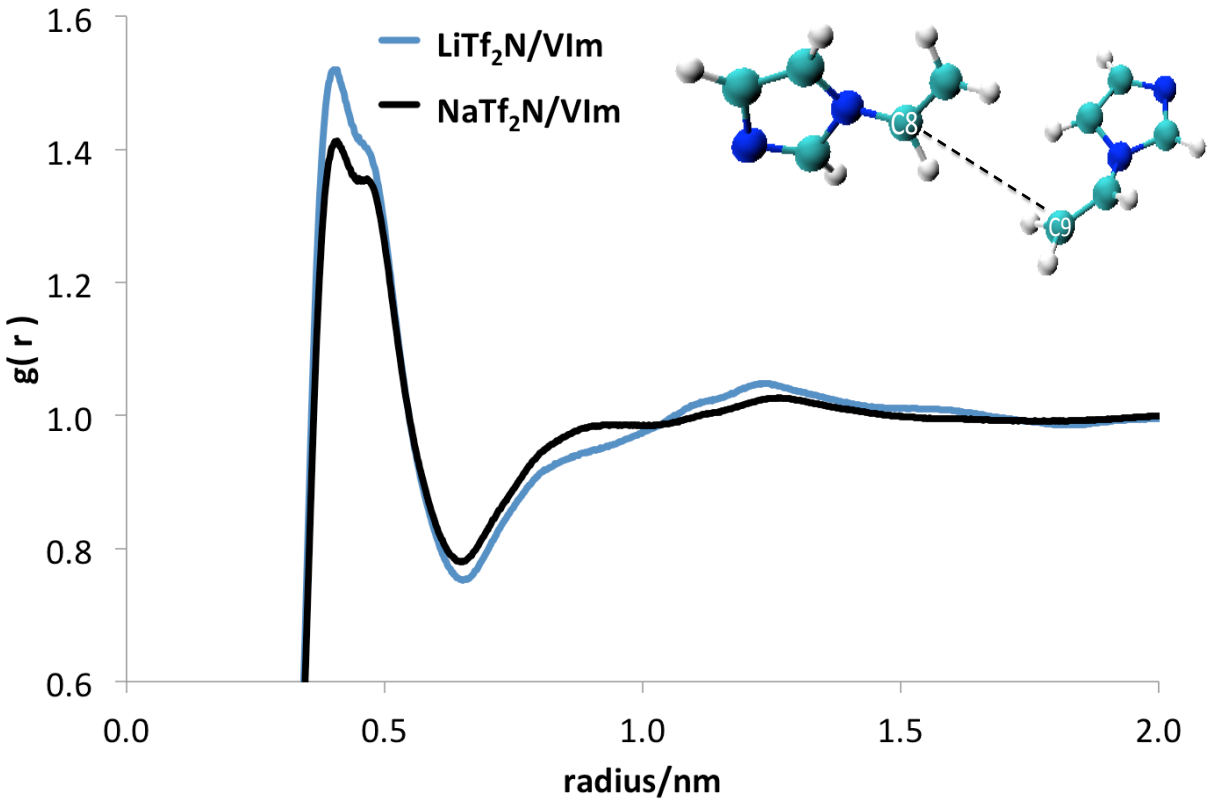

Figure 10. Radial distribution function of C8-C9 atoms of VIm for the 3:1 VIm to IL solutions. The graph shows that mixtures containing Li^+ have a stronger probability of interaction.

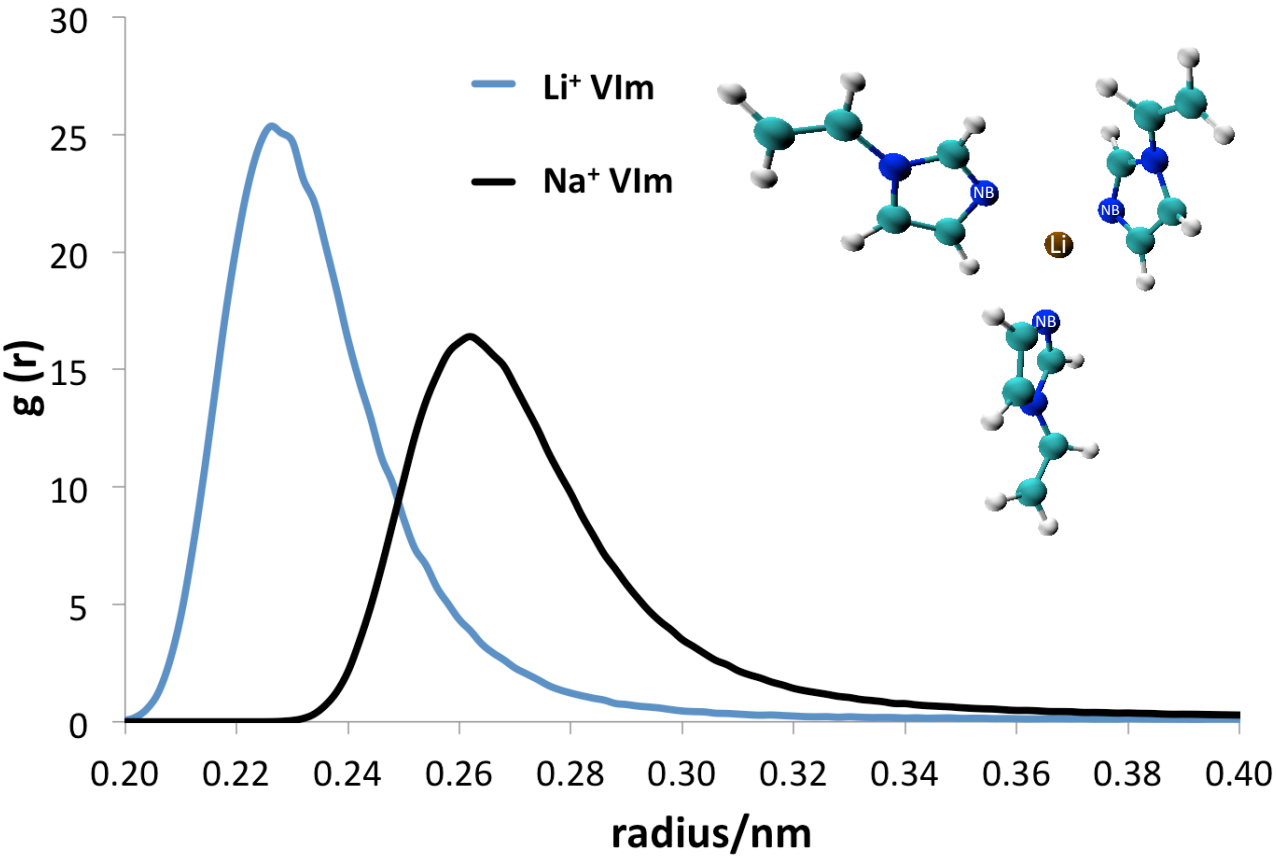

Figure 11. A radial distribution function of the cations (Li^+ and Na^+) and NB atom of VIm for the 3:1 VIm to IL solutions. The graph shows that mixtures containing Li^+ have the a closer interaction with the monomers than Na^+.

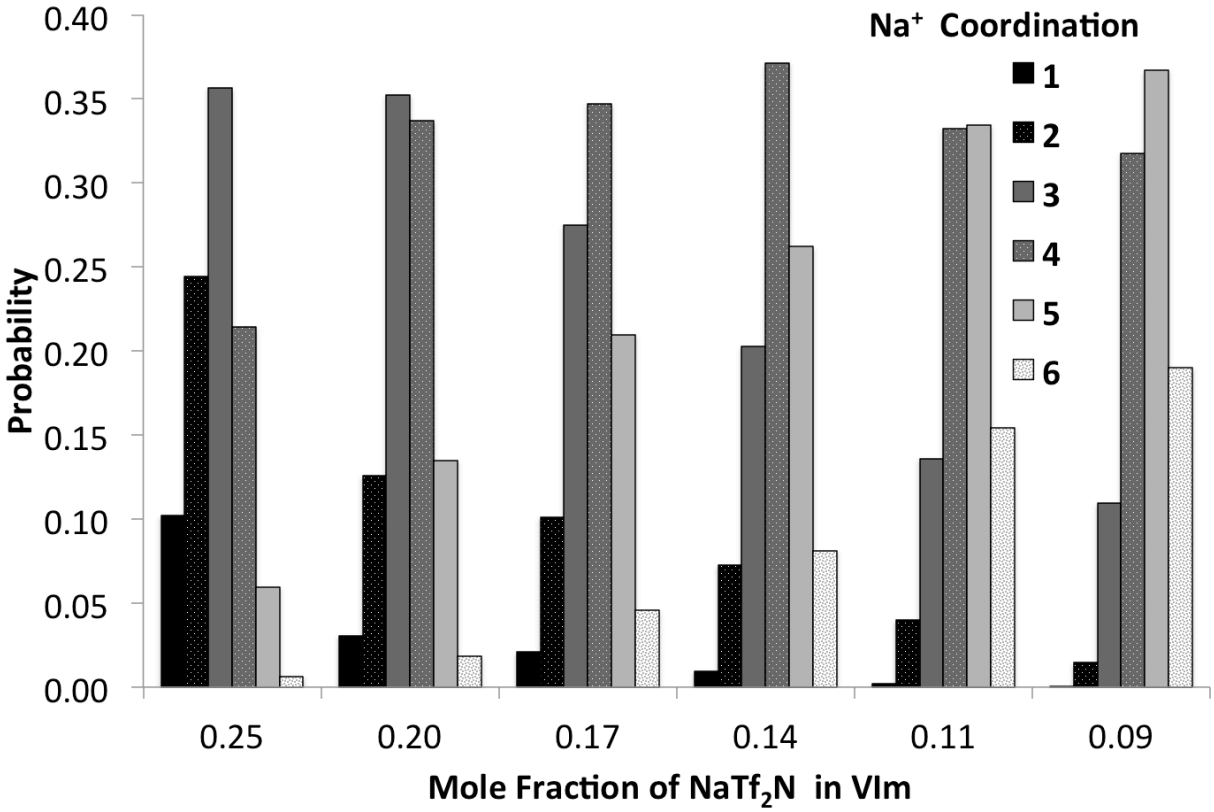

Figure 12. Comparison of the average number of VIm molecules about the Na^+ atom with different mole fractions of $NaTf_2N$ at 303 K.

To explore the effect that different anions might have on the system, two other anions of different size were tested in the same manner as above and used for a comparison. The anions, PF_6^- and BF_4^- were chosen because they are smaller than Tf_2N^-, and they have a high fluorine content (similar to Tf_2N^-). Using the same radial distribution analysis, Figure 13 suggests that while the addition of $LiPF_6$ or $LiBF_4$ improves the local C8-C9 coordination, the probability of finding C8 and C9 in close proximity is still less than that of the mixture of VIm and $LiTf_2N$. This data shows that

there is some correlation between the selected anion and the local concentration of VIm, which is suggested to affect the polymerization behavior of VIm.

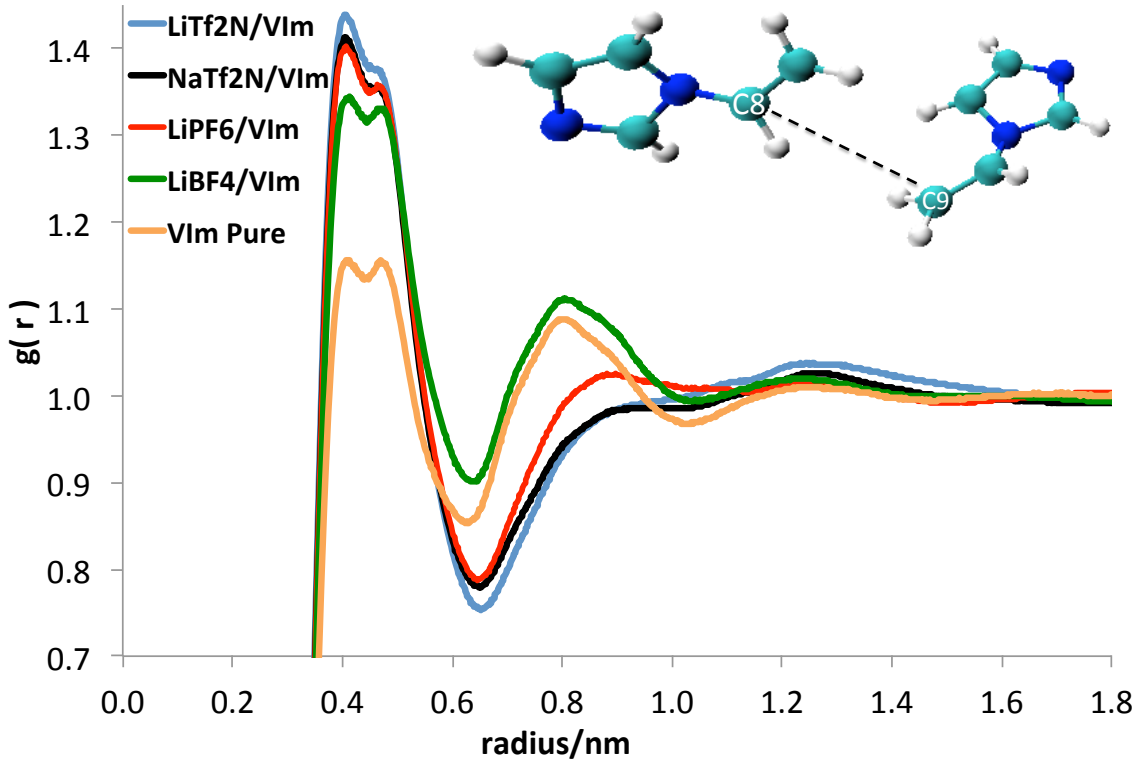

Figure 13. Comparison of radial distribution functions of the C8 and C9 atom of VIm. All mixed solutions have a ratio of 3:1 VIm to IL and are at 303 K.

To further assess the molecular structure in solution, another coordination analysis of VIm about Li^+ was conducted for the mixtures containing PF_6^- and BF_4^- anions. The results of this calculation, shown graphically in Figure 14, indicate that unlike the solutions with $LiTf_2N$, which seem to prefer a coordination of two or three VIm molecules, the VIm monomers in $LiPF_6$ and $LiBF_4$ mixtures appear to have a higher probability of being in a 1:1 ratio of coordination with the Li^+ cation or not coordinated at

all. The reason for this could be that PF_6^- and BF_4^- are more strongly coordinated with Li^+ and hinder the interaction between Li^+ and VIm; however that is not tested in this study.

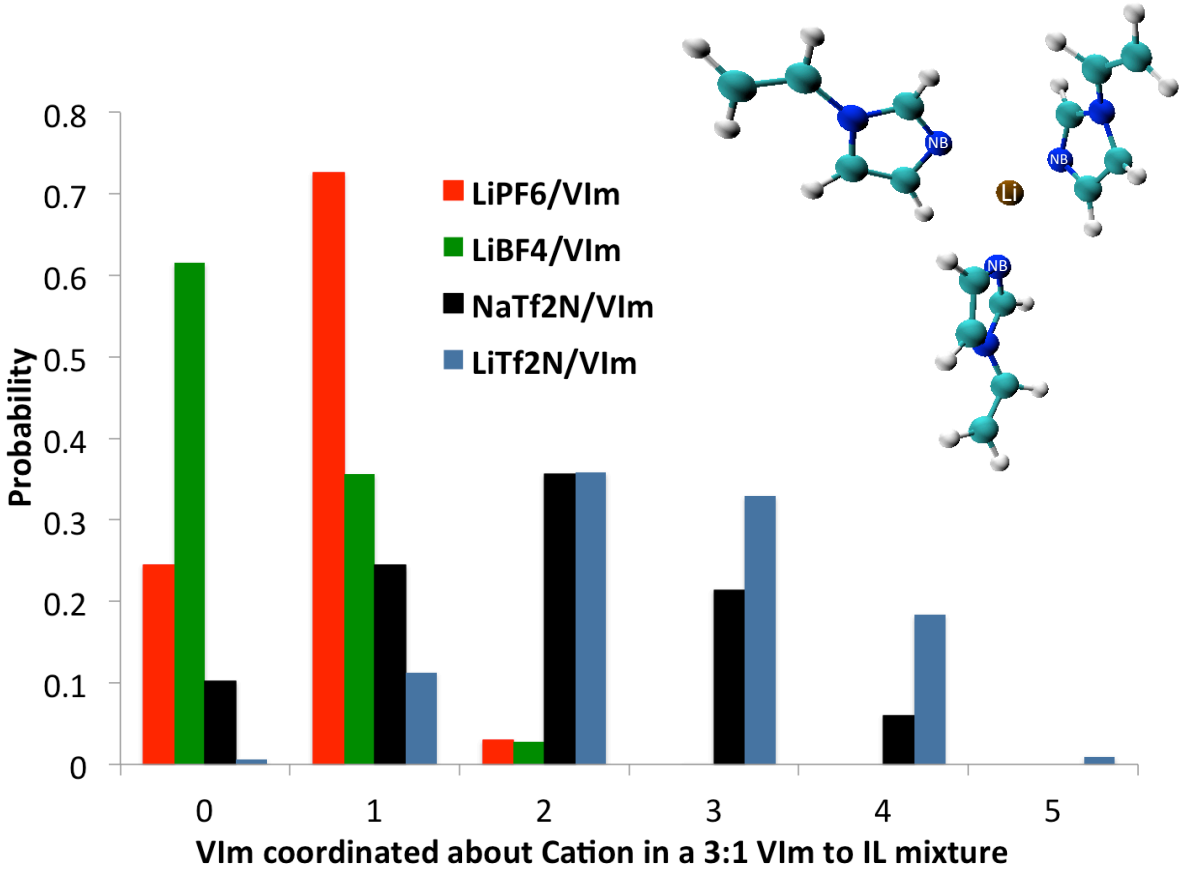

Figure 14. Coordination of VIm to cation probabilities of solutions with different ILs. All solutions in this comparison are at 303K and have a VIm to IL ratio of 3:1.

Chapter 4. Conclusions

We offer molecular-level insight as to why the addition of an ionic liquid consisting of metallic cations and larger weaker coordinating anions significantly increases the polymerization rate and conversion of VIm. Our results show that there are interactions between the metal cations and monomers that cause the monomers to orient in a specific manner related to the IL conformation. After reviewing the data, there is an apparent relationship between the probability of 2:1 VIm-cation interactions and the local concentration of VIm. Although a 2:1 ratio of VIm about the cation seems to aid in the pre-polymerization coordination, the presence of higher ratios might inhibit this favorable coordination. The graphs also distinctly show that as the concentration of IL increases (up to 50%) the local concentration of the vinyl groups increase, directly linking this data to experimental finding and overcoming the mass transport limitation in photopolymerization. In comparison with $LiPF_6$ and $LiBF_4$, mixture solutions containing $LiTf_2N$ were found to have a higher probability of monomers in a favorable coordination for polymerization. While this work does not explicitly show it, it is believed that because Tf_2N^- is a larger molecule, it has a weaker association with its cation than the smaller PF_6^- and BF_4^- molecules. It is believed that this lessened attraction contributes to VIm's ability to coordination around the Li^+ cation. Another possible explanation for the lack of favorable coordination with regards to PF_6^- and BF_4^- relates to the IL's ability to self-

orient in polar and nonpolar regions. It could be that in these mixtures containing ILs, the coordination of VIm is directly linked to how the different cation-anion combinations naturally aggregate in micro-domains. This conclusion, while not answered in this work might offer a deeper understanding into why certain IL combinations aid polymerization while others inhibit it.

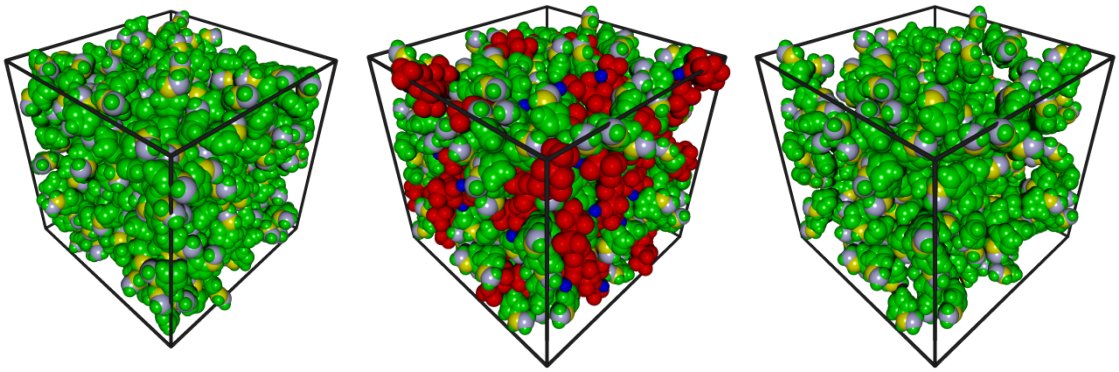

Figure 15. Representative simulation snapshot at 303 K of: (a) pure VIm system; (b) 3:1 molar mixture of VIm:$LiTf_2N$; and (c) 3:1 molar mixture of VIm:$LiTf_2N$, with $LiTf_2N$ molecules removed for clarity.

Figure 15 shows a snapshot of the polar and non-polar regions in 3:1 VIm to $LiTf_2N$ mixture. More work should be focused on the contribution of how the micro-domain segregation of these ionic liquid complexes into polar and non-polar regions affects the coordination of the monomer. Other similar compounds may also demonstrate this behavior, which may contribute to the observed polymerization behavior. A reasonable first step in testing this would be to simulate methyl methacrylate, since these are other studies with this monomer and $LiTf_2N$, under the same conditions as described in this work.[40,46]

Changing the cation of the IL also had an influence over the coordination and local concentration. Despite the stronger coordination that occurs in mixtures with Na^+, VIm interacts with the cation in a similar manner as it does with Li^+. This is most likely why there is only a slight shift in both radial distribution functions and coordination data. It is apparent by the results shown in this work that the addition of ILs similar to $LiTf_2N$ yields a higher local concentration of the polymerizing atoms of VIm. Once again this may be attributed to the IL's inherit nature to aggregate into polar and non-polar regions. In the future this affect will be thoroughly analyzed and quantified.

Chapter 5. Future Work

There is additional modeling work that could be performed on our IL/VIm mixtures in order to provide additional insight. Comparisons with other experimental properties such as the diffusivity of the cation, viscosity, and heat capacity would allow us to further refine the parameters of the simulation models. Previous studies suggest that for most simulation of ionic liquids, these properties will differ from the experimental values by consistent amounts.[66,69] The simulations typically underestimate the diffusivity by two orders of magnitude, while the simulated viscosities tend to overestimate the experimental targets by one order of magnitude.[66] Experimental heat capacity measurements have an approximate 6% margin of error,[70] and the calculated heat capacities often fall within 10-12% of the experimental mean.[66,71] However, at the time of this work, there are no known experimental measures of these additional properties for the $LiTf_2N$/VIm system.

In summary, this simulation study was conducted to provide additional insight into the development of membrane technology for industrial CO_2 separation and capture. It would be interesting to use similar simulation approaches to explore how different alkali Tf_2N additions affect the CO_2 solubility and compare these to CO_2 solubility in imidazolium based organic liquids.[29,31,32] After this, it would be useful to simulate CO_2 permeability, followed by the CO_2/N_2 selectivity of poly-VIm with varying

concentrations of $LiTf_2N$, $NaTf_2N$, KTf_2N, $Mg(Tf_2N)_2$, or combinations of different cations.

References:

1. Kubota, K.; Tamaki, K.; Nohira, T.; Goto, T.; Hagiwara, R. Electrochemical properties of alkali bis(trifluoromethylsulfonyl)amides and their eutectic mixtures. *Electrochimica Acta* 2010, *55* (3), 1113-1119.

2. Bolland, O.; Lindeberg, E. *Power Generation with CO_2 Capture and Sequestration - Research and Fevelopment Needs*; SINTEF Energy Research: Norway, 2000; pp 1-72

3. Moller, F. On Influence of Changes in CO_2 Concentration in Air on Radiation Balance of Earths Surface and on Climate. *Journal of Geophysical Research* 1963, *68* (13), 3877-3886.

4. Watts, R. G. Climate Models and CO_2-Induced Climatic Changes. *Climatic Change* 1980, *2* (4), 387-408.

5. Henrot, A. J.; Francois, L.; Favre, E.; Butzin, M.; Ouberdous, M.; Munhoven, G. Effects of CO2, continental distribution, topography and vegetation changes on the climate at the Middle Miocene: a model study. *Climate of the Past* 2010, *6* (5), 675-694.

6. Wang, Z. H.; Wang, C.; Yin, J. H. Strategies for addressing climate change on the industrial level: affecting factors to CO2 emissions of energy-intensive industries in China. *Natural Hazards* 2015, *75*, S303-S317.

7. Etheridge, D. M.; Steele, L. P.; Langenfelds, R. L.; Francey, R. J.; Barnola, J. M.; Morgan, V. I. Natural and anthropogenic changes in atmospheric CO2 over the last 1000 years from air in Antarctic ice and firn. *Journal of Geophysical Research-Atmospheres* 1996, *101* (D2), 4115-4128.

8. *Inventory of U.S. Greenhouse Gas Emissions and Sinks: 1990-2012*; Environmental Protection Agency: Washington DC, 2015; pp 1-27.

9. Singer, J. *Combustion Fossil Power*. Fouth ed.; Combustion Engineering Inc.: Windsor, Connecticut, 1991.

10. Nordhaus, W. D. To Slow or Not to Slow: The Econimics of the Greenhouse Effect. *Economic Journal* 2015, *125* (583), 603-620.

11. Standards of Performance for Greenhouse Gas Emissions from Existing Sources: Electric Utility Generating Units. In *40 CFR 60*, Agency, E. P., Ed. Washington DC, 2014; Vol. 2014-26112, pp 34829 -34958.
12. Plasynski, S. I.; Chen, Z. Y. Review of CO2 capture technologies and some improvement opportunities. *Abstracts of Papers of the American Chemical Society* 2000, *220*, U391-U391.

13. Herzog, H. J.; Golomb, D. Carbon capture and storage from fossil fuel use. *Encyclopedia of energy, Elsevier Science* 2004, 277-287.

14. Meisen, A.; Shuai, X. S. Research and development issues in CO2 capture. *Energy Conversion and Management* 1997, *38*, S37-S42.

15. Universal Industrial Gases, I. Overview of Cryogenic Air Separation and Liquefier Systems. http://www.uigi.com/cryodist.html (accessed 06/01/2015).

16. Mondal, M. K.; Balsora, H. K.; Varshney, P. Progress and trends in CO2 capture/separation technologies: A review. *Energy* 2012, *46* (1), 431-441.

17. Yu, C. H.; Huang, C. H.; Tan, C. S. A Review of CO2 Capture by Absorption and Adsorption. *Aerosol and Air Quality Research* 2012, *12* (5), 745-769.

18. Samanta, A.; Zhao, A.; Shimizu, G. K. H.; Sarkar, P.; Gupta, R. Post-Combustion CO2 Capture Using Solid Sorbents: A Review. *Industrial & Engineering Chemistry Research* 2012, *51* (4), 1438-1463.

19. Wong, S.; Bioletti, R. Carbon Dioxide Separation Technologies. Alberta Research Council: Alberta, Canada, 2002; pp 1-14.

20. Babcock & Wilcox Power Generation Group, I. Wet Flue Gas Desulfurization (FGD) Systems Advanced Multi-Pollutant Control Technology. http://www.babcock.com/library/documents/e1013167.pdf (accessed 05/20/2015).

21. FlowVision. SCR DeNOx Technology. http://www.flowvision-energy.com/scr-denox-tech (accessed 05/20/2015).

22. Leifsen, H. Post-Combustion CO2 Capture Using Chemical Absorption. Norwegian University of Science and Technology, Norway, 2007.

23. Gottlicher, G.; Pruschek, R. Comparison of CO2 removal systems for fossil-fueled power plant processes. *Energy Conversion and Management* 1997, *38*, S173-S178.

24. Wilkes, J. S. A short history of ionic liquids - from molten salts to neoteric solvents. *Green Chemistry* 2002, *4* (2), 73-80.

25. Ghandi, K. A Review of Ionic Liquids, Their Limits and Applications. *Green and Sustainable Chemistry* 2014, *4* (1), 44-53.
26. Maginn, E. J. Atomistic Simulation of Ionic Liquids. In *Reviews in Computational Chemistry*, Lipkowitz, K.; Cundari, T., Eds. John and Wiley Inc.: New York, 2009; Vol. 26, pp 421-493.

27. Vila, J.; Gines, P.; Rilo, E.; Cabeza, O.; Varela, L. M. Great increase of the electrical conductivity of ionic liquids in aqueous solutions. *Fluid Phase Equilibria* 2006, *247* (1-2), 32-39.

28. Sangoro, J. R.; Iacob, C.; Agapov, A. L.; Wang, Y.; Berdzinski, S.; Rexhausen, H.; Strehmel, V.; Friedrich, C.; Sokolov, A. P.; Kremer, F. Decoupling of ionic conductivity from structural dynamics in polymerized ionic liquids. *Soft Matter* 2014, *10* (20), 3536-3540.

29. Cadena, C.; Anthony, J. L.; Shah, J. K.; Morrow, T. I.; Brennecke, J. F.; Maginn, E. J. Why is CO2 so soluble in imidazolium-based ionic liquids? *Journal of the American Chemical Society* 2004, *126* (16), 5300-5308.

30. Gonzalez-Miquel, M.; Palomar, J.; Omar, S.; Rodriguez, F. CO2/N-2 Selectivity Prediction in Supported Ionic Liquid Membranes (SILMs) by COSMO-RS. *Industrial & Engineering Chemistry Research* 2011, *50* (9), 5739-5748.

31. Hu, X. D.; Tang, J. B.; Blasig, A.; Shen, Y. Q.; Radosz, M. CO2 permeability, diffusivity and solubility in polyethylene glycol-grafted polyionic membranes and their CO2 selectivity relative to methane and nitrogen. *Journal of Membrane Science* 2006, *281* (1-2), 130-138.

32. Bara, J. E.; Gabriel, C. J.; Hatakeyama, E. S.; Carlisle, T. K.; Lessmann, S.; Noble, R. D.; Gin, D. L. Improving CO2 selectivity in polymerized room-temperature ionic liquid gas separation membranes through incorporation of polar substituents. *Journal of Membrane Science* 2008, *321* (1), 3-7.

33. Yildiz, G.; Oztekin, N.; Orbay, A.; Senkal, F. Voltammetric determination of nitrite in meat products using polyvinylimidazole modified carbon paste electrode. *Food Chemistry* 2014, *152*, 245-250.

34. MacAodha, D.; Conghaile, P. O.; Egan, B.; Kavanagh, P.; Leech, D. Membraneless Glucose/Oxygen Enzymatic Fuel Cells Using Redox Hydrogel Films Containing Carbon Nanotubes. *Chemphyschem* 2013, *14* (10), 2302-2307.

35. Farjaminezhad, M.; Tehrani, M. S.; Azar, P. A.; Hussain, S. W.; Bohlooli, S. Polyvinylimidazole/sol-gel composite as a novel solid-phase microextraction coating for the determination of halogenated benzenes from aqueous solutions. *Journal of Separation Science* 2014, *37* (12), 1475-1481.

36. Corazza, M. Z.; Ribeiro, E. S.; Segatelli, M. G.; Tarley, C. R. T. Study of cross-linked poly(methacrylic acid) and polyvinylimidazole as selective adsorbents for on-line preconcentration and redox speciation of chromium with flame atomic absorption spectrometry determination. *Microchemical Journal* 2014, *117*, 18-26.

37. Wang, R. X.; Men, J. Y.; Gao, B. J. The Adsorption Behavior of Functional Particles Modified by Polyvinylimidazole for Cu(II) Ion. *Clean-Soil Air Water* 2012, *40* (3), 278-284.

38. Whitley, J. W.; Home, W. J.; Danielsen, S. P. O.; Shannon, M. S.; Marshall, J. E.; Hayward, S. H.; Gaddis, C. J.; Bara, J. E. Enhanced photopolymerization rate & conversion of 1-vinylimidazole in the presence of lithium bistriflimide. *European Polymer Journal* 2014, *60*, 92-97.

39. Zhou, H.; Jimenez, Z.; Pojman, J. A.; Paley, M. S.; Hoyle, C. E. Photopolymerization kinetics of tributylmethylammonium-based (meth)acrylate ionic liquids and the effect of water. *Journal of Polymer Science Part a-Polymer Chemistry* 2008, *46* (11), 3766-3773.

40. Noble, B. B.; Smith, L. M.; Coote, M. L. The effect of LiNTf2 on the propagation rate coefficient of methyl methacrylate. *Polymer Chemistry* 2014, *5* (17), 4974-4983.

41. Gromov, V. F.; Osmanov, T. O.; Khomikovskii, P. M.; Abkin, A. D. Polymerization of Acrylamide in Various Solvents in the Presence of Lewis-Acids. *European Polymer Journal* 1980, *16* (9), 803-808.

42. Bamford, C. H.; Jenkins, A. D.; Johnston, R. Studies in Polymerization .12. Salt Effects on the Polymerization of Acrylonitrile in Non-Aqueous Solution. *Proceedings of the Royal Society of London Series a-Mathematical and Physical Sciences* 1957, *241* (1226), 364-375.

43. Pedron, S.; Guzman, J.; Garcia, N. Polymerization Kinetics of Ethylene Oxide Methacrylates in Ionic Media. *Macromolecular Chemistry and Physics* 2011, *212* (8), 860-869.

44. Hermosilla, L.; Calle, P.; Tiemblo, P.; Garcia, N.; Garrido, L.; Guzman, J. Polymerization of Methyl Methacrylate with Lithium Triflate. A Kinetic and Structural Study. *Macromolecules* 2013, *46* (14), 5445-5454.

45. Kubisa, P. Ionic liquids as solvents for polymerization processes-Progress and challenges. *Progress in Polymer Science* 2009, *34* (12), 1333-1347.

46. Matsumoto, A.; Nakamura, S. Radical polymerization of methyl methacrylate in the presence of magnesium bromide as the Lewis acid. *Journal of Applied Polymer Science* 1999, *74* (2), 290-296.

47. Tazuke, S.; Okamura, S. Effects of Metal Salts on Polymerization .6. Photo and Thermally Catalyzed Polymerization of N-vinylimidazole in Presence of Metal Salts. *Journal of Polymer Science Part a-1-Polymer Chemistry* 1969, *7* (3PA1), 851-864.

48. Li, Z.; Smith, G. D.; Bedrov, D. Li+ Salvation and Transport Properties in Ionic Liquid/Lithium Salt Mixtures: A Molecular Dynamics Simulation Study. *Journal of Physical Chemistry B* 2012, *116* (42), 12801-12809.

49. Haskins, J. B.; Bennett, W. R.; Wu, J. J.; Hernandez, D. M.; Borodin, O.; Monk, J. D.; Bauschlicher, C. W.; Lawson, J. W. Computational and Experimental Investigation of Li-Doped Ionic Liquid Electrolytes: pyr14 TFSI , pyr13 FSI , and EMIM BF4. *Journal of Physical Chemistry B* 2014, *118* (38), 11295-11309.

50. Hayamizu, K.; Tsuzuki, S.; Seki, S.; Fujii, K.; Suenaga, M.; Umebayashi, Y. Studies on the translational and rotational motions of ionic liquids composed of N-methyl-N-propyl-pyrrolidinium (P-13) cation and bis(trifluoromethanesulfonyl)amide and bis(fluorosulfonyl)amide anions and their binary systems including lithium salts. *Journal of Chemical Physics* 2010, *133* (19), 194505.

51. Hess, B.; Kutzner, C.; van der Spoel, D.; Lindahl, E. GROMACS 4: Algorithms for highly efficient, load-balanced, and scalable molecular simulation. *Journal of Chemical Theory and Computation* 2008, *4* (3), 435-447.

52. Parrinello, M.; Rahman, A. Crystal-Structure and Pair Potnetials- A Molecular-Dynamics Study. *Physical Review Letters* 1980, *45* (14), 1196-1199.

53. Hoover, W. G. Canonical Dynamics - Equilibrium Phase-Space Distributions. *Physical Review A* 1985, *31* (3), 1695-1697.

54. Essmann, U.; Perera, L.; Berkowitz, M. L.; Darden, T.; Lee, H.; Pedersen, L. G. A Smooth Particle Mesh Ewald Method. *Journal of Chemical Physics* 1995, *103* (19), 8577-8593.

55. Allen, M. P.; Tildesley, D. J. *Computer Simulation of Liquids*. Oxford University Press: Oxford, UK, 1989.

56. Jorgensen, W. L.; Maxwell, D. S.; TiradoRives, J. Development and testing of the OPLS all-atom force field on conformational energetics and properties of organic liquids. *Journal of the American Chemical Society* 1996, *118* (45), 11225-11236.

57. Lopes, J. N. C.; Padua, A. A. H. Molecular force field for ionic liquids composed of triflate or bistriflylimide anions. *Journal of Physical Chemistry B* 2004, *108* (43), 16893-16898; Carignano, M. A. Structure and Dynamics of PF6 P-1,P-2,P-2,P-4 from Molecular Dynamics Simulations. *Journal of Physical Chemistry B* 2013, *117* (48), 15176-15183.

58. Shim, Y.; Choi, M. Y.; Kim, H. J. A molecular dynamics computer simulation study of room-temperature ionic liquids. II. Equilibrium and nonequilibriurn solvation dynamics. *Journal of Chemical Physics* 2005, *122* (4), 12, 044511.

59. Frisch, M. J.; Trucks, G. W.; Schlegel, H. B.; Scuseria, G. E.; Robb, M. A.; Cheeseman, J. R.; Scalmani, G.; Barone, V.; Mennucci, B.; Petersson, G. A.; Nakatsuji, H.; Caricato, M.; Li, X.; Hratchian, H. P.; Izmaylov, A. F.; Bloino, J.; Zheng, G.; Sonnenberg, J. L.; Hada, M.; Ehara, M.; Toyota, K.; Fukuda, R.; Hasegawa, J.; Ishida, M.; Nakajima, T.; Honda, Y.; Kitao, O.; Nakai, H.; Vreven, T.; Montgomery, J. A., Jr.; Peralta, J. E.; Ogliaro, F.; Bearpark, M.; Heyd, J. J.; Brothers, E.; Kudin, K. N.; Staroverov, V. N.; Kobayashi, R.; Normand, J.; Raghavachari, K.; Rendell, A.; Burant, J. C.; Iyengar, S. S.; Tomasi, J.; Cossi, M.; Rega, N.; Millam, M. J.; Klene, M.; Knox, J. E.; Cross, J. B.; Bakken, V.; Adamo, C.; Jaramillo, J.; Gomperts, R.; Stratmann, R. E.; Yazyev, O.; Austin, A. J.; Cammi, R.; Pomelli, C.; Ochterski, J. W.; Martin, R. L.; Morokuma, K.; Zakrzewski, V. G.; Voth, G. A.; Salvador, P.; Dannenberg, J. J.; Dapprich, S.; Daniels, A. D.; Farkas, Ö.; Foresman, J. B.; Ortiz, J. V.; Cioslowski, J.; Fox, D. J. Gaussian 09. Gaussian, Inc.: Wallingford CT, 2009.

60. Becke, A. D. Density-functional thermochemistry. III. The role of exact exchange. *J. Chem. Phys.* 1993, *98,* 5648-5652.

61. Reed, A. E.; Curtiss, L. A.; Weinhold, F. Intermolecular Interactions From A Natural Bond Orbital, Donor-Acceptor Viewpoint. *Chemical Reviews* 1988, *88* (6), 899-926.

62. Zhang, Y.; Maginn, E. J. A Simple AIMD Approach to Derive Atomic Charges for Condensed Phase Simulation of Ionic Liquids. *Journal of Physical Chemistry B* 2012, *116* (33), 10036-10048.

63. Zhao, W.; Eslami, H.; Cavalcanti, W. L.; Mueller-Plathe, F. A refined all-atom model for the ionic liquid 1-n-butyl 3-methylimidazolium bis(trifluoromethylsulfonyl)imide bmim Tf2N. *Zeitschrift Fur Physikalische Chemie-International Journal of Research in Physical Chemistry & Chemical Physics* 2007, *221* (11-12), 1647-1662.

64. Mendez-Morales, T.; Carrete, J.; Bouzon-Capelo, S.; Perez-Rodriguez, M.; Cabeza, O.; Gallego, L. J.; Varela, L. M. MD Simulations of the Formation of Stable Clusters in Mixtures of Alkaline Salts and Imidazolium-Based Ionic Liquids. *Journal of Physical Chemistry B* 2013, *117* (11), 3207-3220.

65. Marczewski, M. J.; Stanje, B.; Hanzu, I.; Wilkening, M.; Johansson, P. "Ionic liquids-in-salt" - a promising electrolyte concept for high-temperature lithium batteries? *Physical Chemistry Chemical Physics* 2014, *16* (24), 12341-12349.

66. Liu, H. J.; Maginn, E.; Visser, A. E.; Bridges, N. J.; Fox, E. B. Thermal and Transport Properties of Six Ionic Liquids: An Experimental and Molecular Dynamics Study. *Industrial & Engineering Chemistry Research* 2012, *51* (21), 7242-7254.

67. Stilling.Fh; Rahman, A. Improved Simulation of Liquid Water By Molecular-Dynamics. *Journal of Chemical Physics* 1974, *60* (4), 1545-1557.

68. Metallic, Covalent and Ionic Radii. http://www.wiredchemist.com/chemistry/data/metallic-radii (accessed 06/05/2015).

69. Ghatee, M. H.; Zare, M.; Moosavi, F.; Zolghadr, A. R. Temperature-Dependent Density and Viscosity of the Ionic Liquids 1-Alkyl-3-methylimidazolium Iodides: Experiment and Molecular Dynamics Simulation. *Journal of Chemical and Engineering Data* 2010, *55* (9), 3084-3088.

70. Chirico, R. D.; Diky, V.; Magee, J. W.; Frenkel, M.; Marsh, K. N. Thermodynamic and Thermophysical Properties of the Reference Ionic Liquid: 1-hexel-3-methylimidazolium bis (trifluoromethyl)sulfonyl amide (Including Mixtures). Part 2. Critical Evaluation and Recommended Property Values (IUPAC Technical Report). *Pure and Applied Chemistry* 2009, *81* (5), 791-828.

71. Chen, M.; Pendrill, R.; Widmalm, G.; Brady, J. W.; Wohlert, J. Molecular Dynamics Simulations of the Ionic Liquid 1-n-Butyl-3-Methylimidazolium Chloride and Its Binary Mixtures with Ethanol. *Journal of Chemical Theory and Computation* 2014, *10* (10), 4465-4479.

Appendix A: Exploration of Other Cations

In order to broaden our investigation and explore the role of other cations for alkali Tf_2N solvents on the VIm pre-polymerization structure, two other ILs with metallic cations were considered: KTf_2N, and $Mg(Tf_2N)_2$. Since experimental data was available in literature,[1] the simulated densities of pure KTf_2N were compared to experimental data before analyzing the coordination effects.

Before coordination calculations and radial distribution functions were calculated, the parameters KTf_2N were optimized to have densities that were similar to experimental densities. The model of KTf_2N with no charge or Lennard Jones scaling, yielded simulated densities that were within a reasonable margin of error. In fact, applying the same conditions that were applied to Li^+ and Na^+ pushed the simulation densities out of the range of acceptable error for predictive methods. Instead, the only modification that was made to the KTf_2N parameters was a charge scaling of 0.95. This strengthened the correlation between simulation and experimental densities significantly as shown in Figure A1.

When benchmarking $LiTf_2N$ and $NaTf_2N$ there was a subtle trend between the size of the cation and the error of the density. If left unmodified (using OPLS parameters for the cations and those proposed by Zhao et al. for Tf_2N^-), the trend shows that as the cations decrease in size, the simulation density increases in error. One possible

explanation is that there is a fundamental error in parameter for modeling ionic systems such as these with simple fixed charge models. However, since this work focuses on the structural orientation only of these systems, benchmarking these simulations to experimental densities should be sufficient enough to gain some qualitative insight about the molecules behavior regardless if scaling schemes are somewhat different.

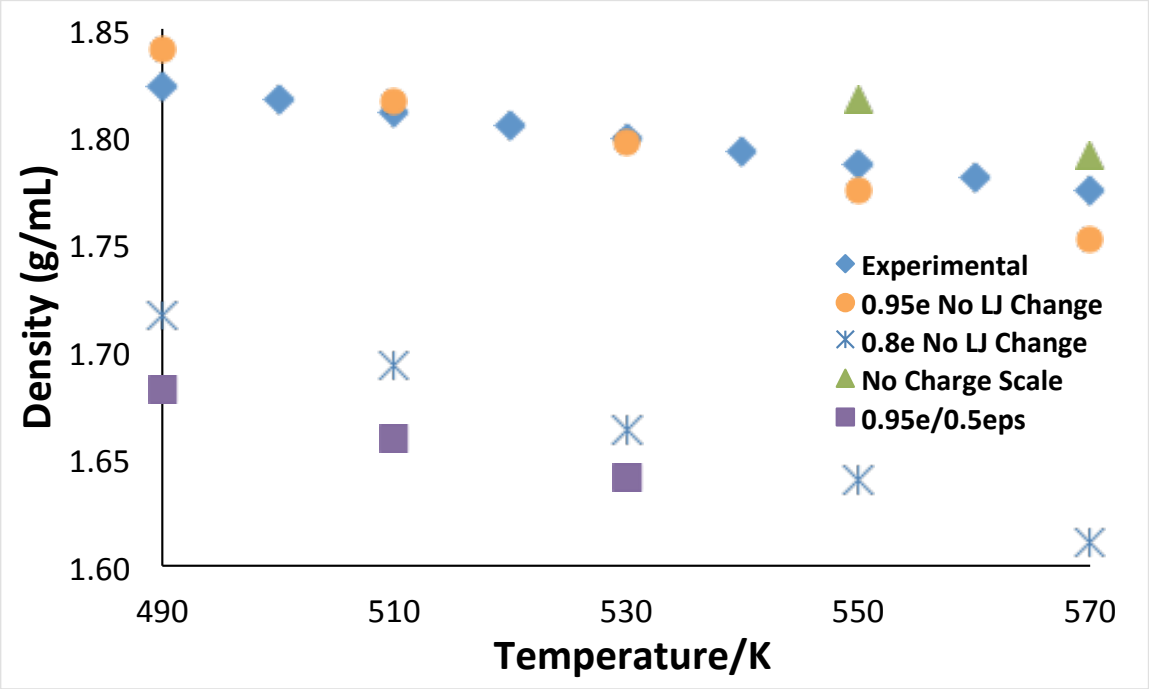

Figure A1. Comparison of experimental and simulation density profile with respect to varying temperatures for which KTf_2N is in the liquid state. The graph shows that a good agreement between simulation and experimental density can be achieved when partial charges are scaled by a factor of 0.95. A scale of 0.8 for charges yields a density that is much too low.

Experimental densities for liquid $Mg(Tf_2N)_2$ were unable to be located, so there was no benchmarking conducted. However, given the assumption above it seemed reasonable to treat $Mg(Tf_2N)_2$ similarly to $NaTf_2N$ given that Mg^{2+} and Na^{+} are similar in size. The charges were scaled by 0.8 and sigma was scaled by 1.05.

As observed with the Li^+ cation, VIm seems to form a complex with all metal cations tested but to different degrees. Coordination calculations show that Mg^{2+} has a VIm coordination similar to Li^+. Figure A2 shows that Mg^{2+} has the same 2:1 metal to VIm tendency, except that the system with $MgTf_2N$ holds this confirmation as the most probable at higher VIm concentrations.

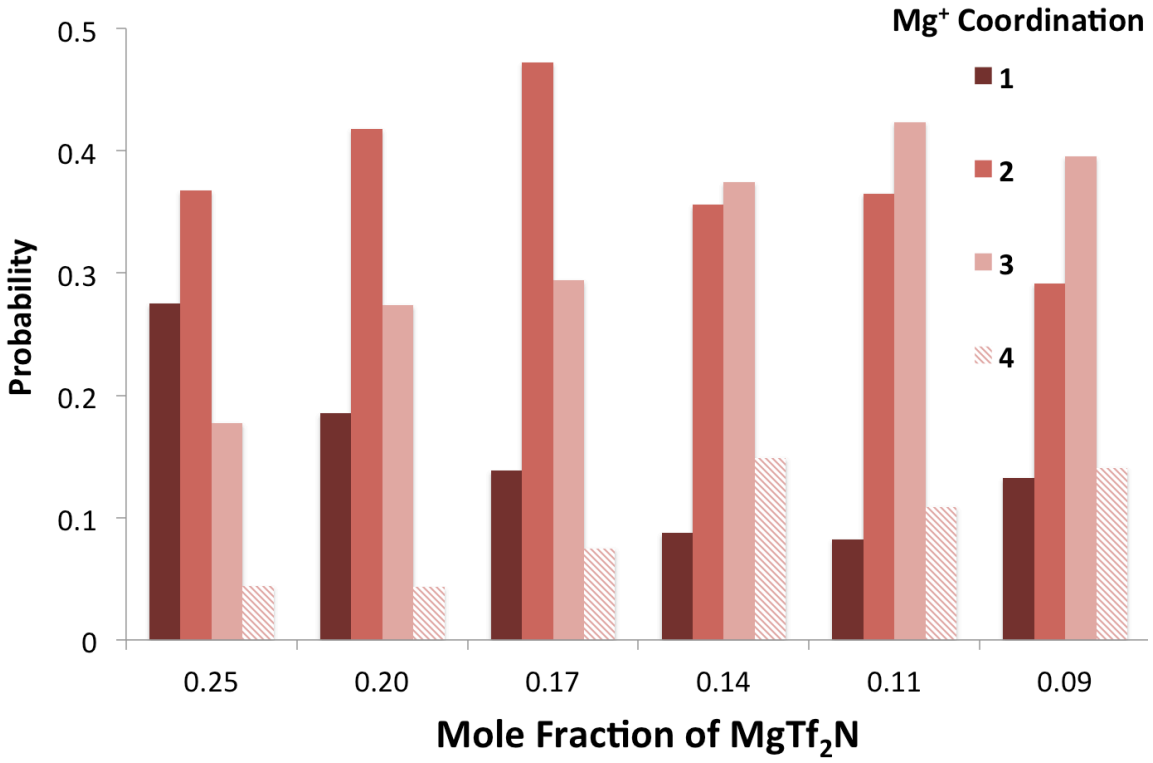

Figure A2 Coordination probabilities of solutions with different VIm $Mg(Tf_2N)_2$ ratios at 303K. The plot above shows that the coordination is similar to that of Li – VIm coordinations, with the exception that the 2:1 interaction becomes more probable at higher VIm concentrations.

With KTf_2N additions, there is a higher probability of finding a greater number of VIm coordinated about the metal cation. Figures A3 shows that for K mixtures, coordinations of 4:1 and 5:1 are favored as VIm concentration increases. Analysis and comparison of this data with that of $LiTf_2N$, $LiPF_6$, and $LiBF_4$ suggest that the preferred

interaction to increase local concentration of VIm in a favorable confirmation is a 2:1 monomer to metal interaction. Figure A4 shows the radial distribution of the C9 atom about the C8 atom, the vinyl group where polymerization takes place. The graph shows that all IL additions increase local concentration. However, mixtures including $Mg(Tf_2N)_2$ yield a much higher g(r) than other metal cations tested.

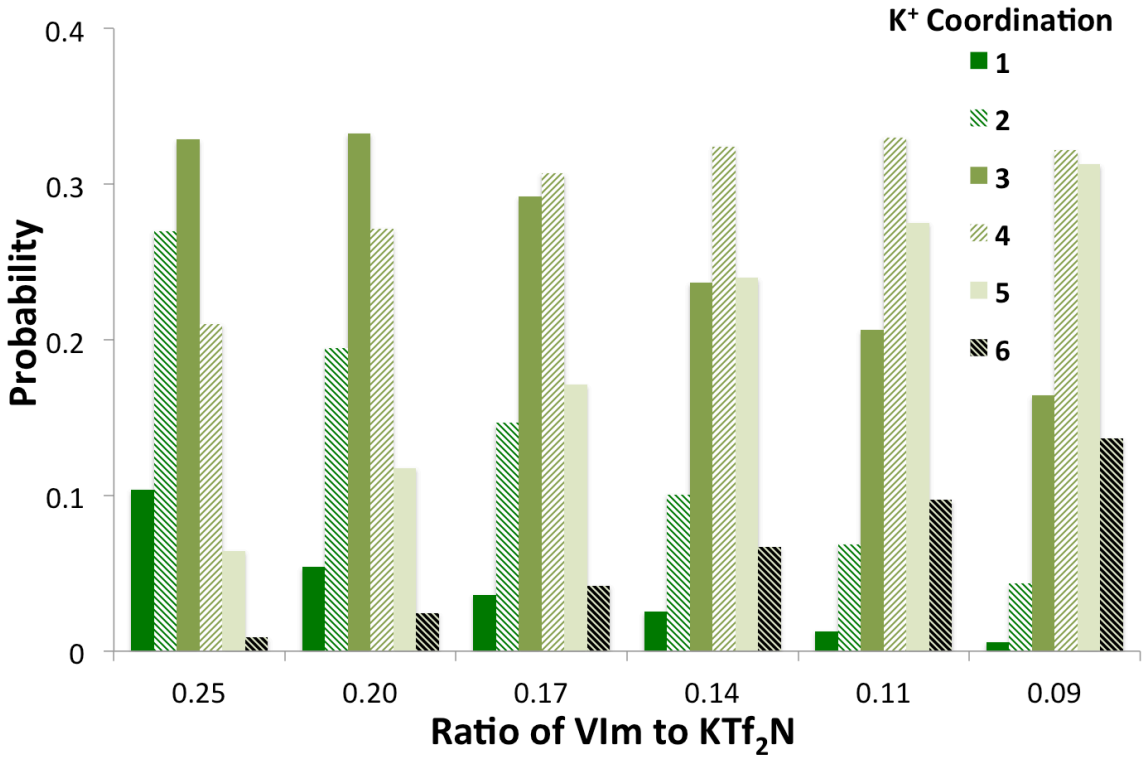

Figure A3 Coordination probabilities of solutions of solutions with different VIm to KTf_2N ratios at 303K. The plot above shows VIm found to have coordinated around the larger K cation in ratios of 4:1 and greater.

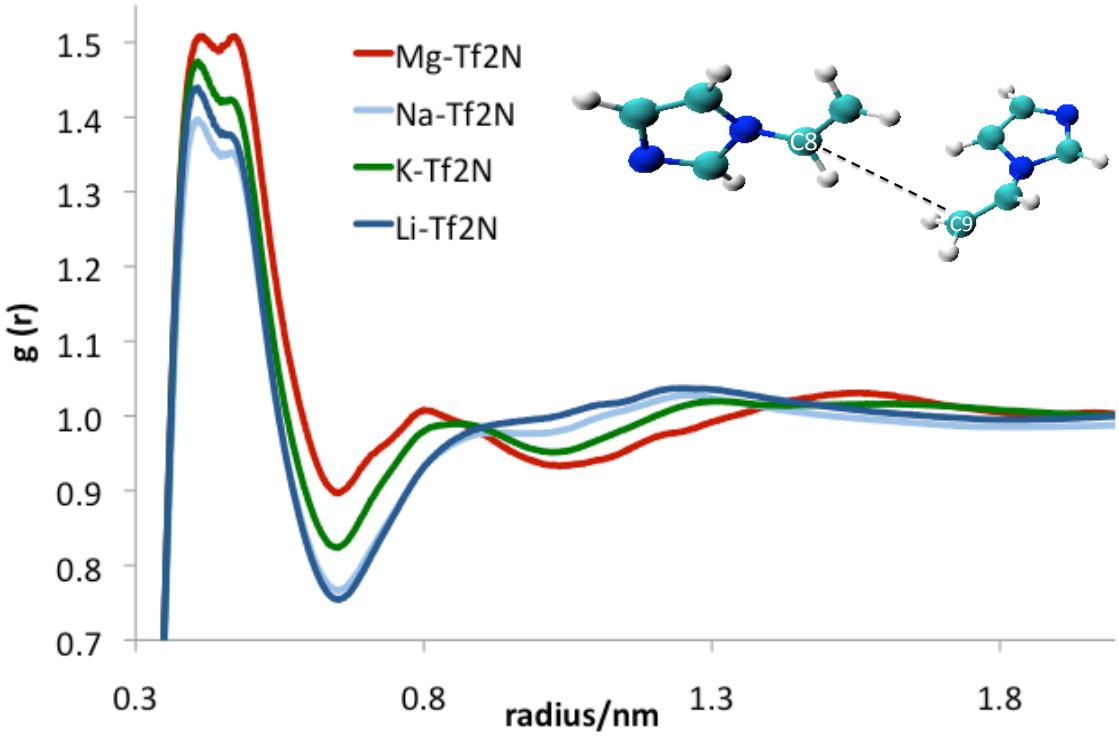

Figure A4 Radial distribution function of C8-C9 atoms of VIm for the 3:1 VIm to IL solutions. The graph shows that mixtures containing Mg^{2+} have a stronger probability of favorable confirmation.

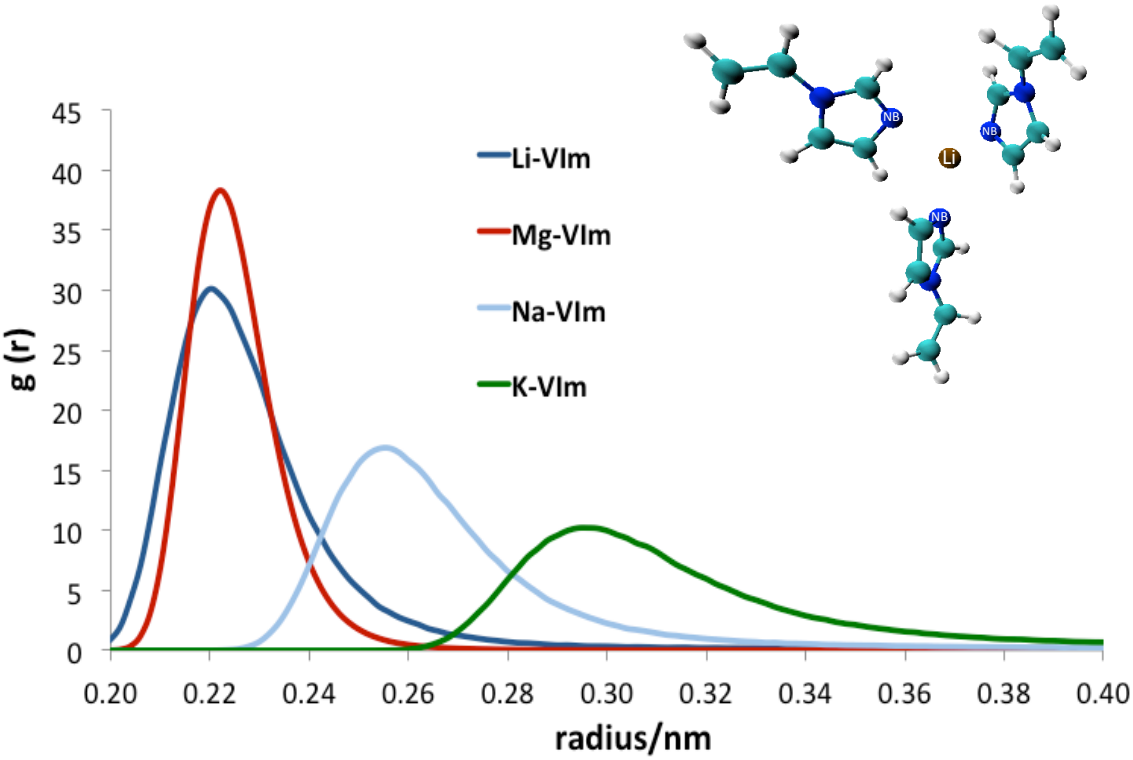

Figure A5 Radial distribution function of Cation and NB atom of VIm for the 3:1 VIm to IL solutions. The graph shows that mixtures containing Li^+ and Mg^{2+} have a closer interaction with the monomers than Na^+ or K^+.

Appendix B: Further Refinement of Parameters

In an attempt to further refine the parameters of the $LiTf_2N$ in VIm system, several other schemes were attempted to scale the Lennard Jones parameters.

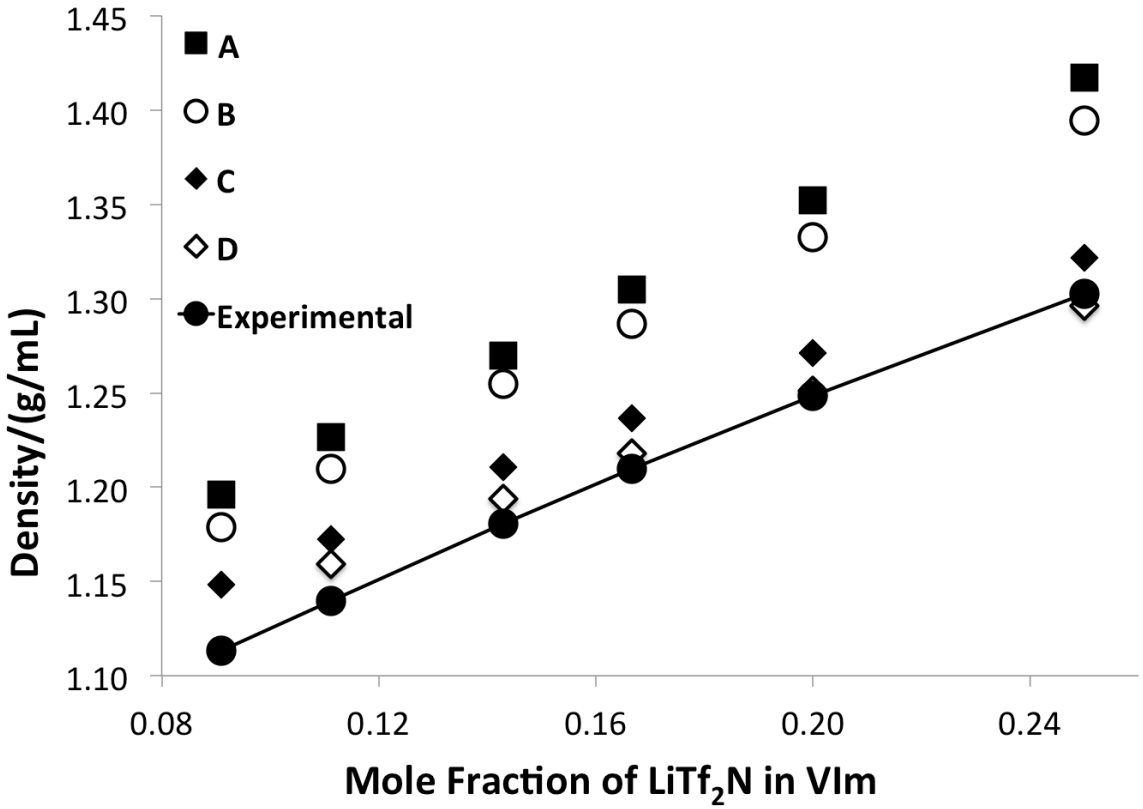

Figure B1. Density comparison of different Lennard-Jones sigma scaling between the VIm and $LiTf_2N$ interactions. **A.** No Lennard Jones scaling. **B.** only $LiTf_2N$ interactions scaled in accordance with Table 3. **C.** 1.08 σ only. **D.**(open diamond) 1.1 σ only

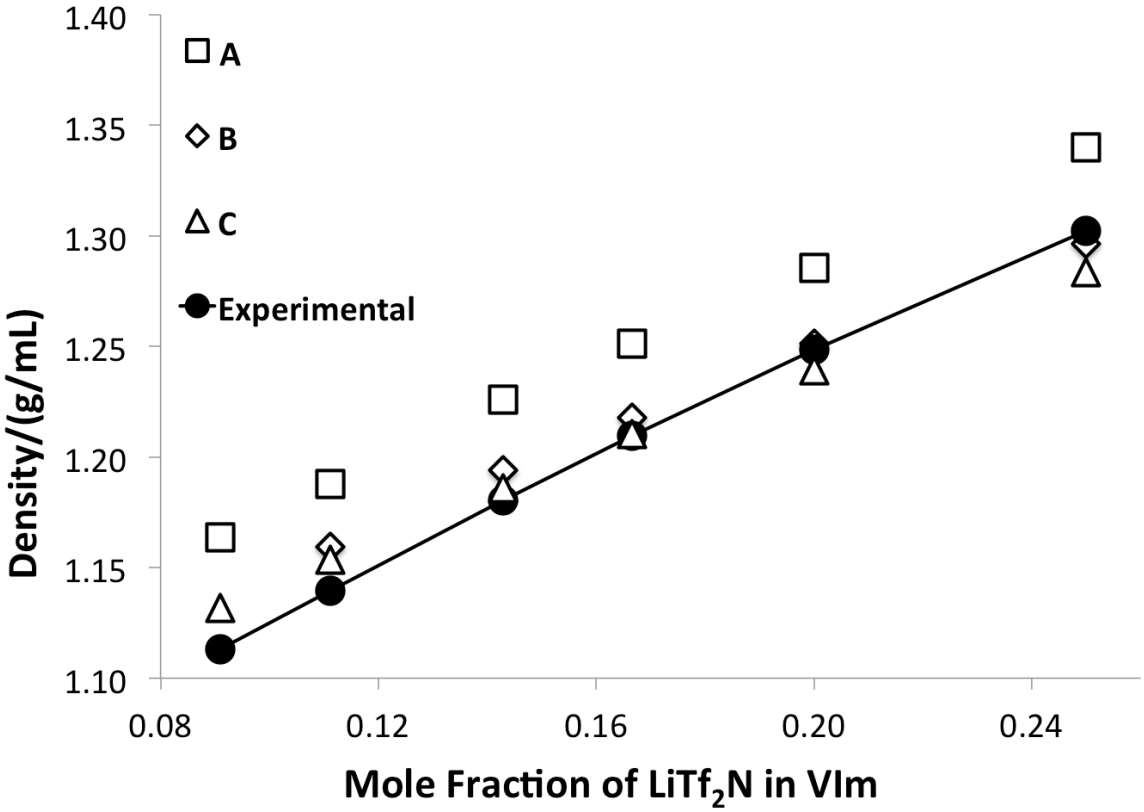

Figure B2. Density comparison of different Lennard-Jones epsilon scaling between the VIm and $LiTf_2N$ interactions. **A.** 1.5 ε and 1.1 σ **B.** 1.1 σ only. **C**. 0.5 ε and 1.1 σ .

Figure B1 shows the comparison of densities for different Lennard Jones sigma scales, and Fiure B2 shows the comparison of densities for different Lennard Jones epsilon scales. With the exception of trend **A** in Figure B1, the interactions between Li^+ and Tf_2N^- had σ scaled by 1.05 just as described in Chapter 3.1 of this work.